Master's Thesis

Study on Swirl and Cross Flow of 3D-Printed Rotational Mixing Vane in 2×3 Subchannel

Haneol Park

Department of Nuclear Engineering

Graduate School of UNIST

2019

Study on Swirl and Cross Flow of 3D-Printed Rotational Mixing Vane in 2×3 Subchannel

Haneol Park

Department of Nuclear Engineering

Graduate School of UNIST

Study on Swirl and Cross Flow of 3D-Printed Rotational Mixing Vane in 2×3 Subchannel

A thesis/dissertation
submitted to the Graduate School of UNIST
in partial fulfillment of the
requirements for the degree of
Master of Science

Haneol Park

07/09/2019
Approved by

_____

Advisor
In Cheol Bang

Study on Swirl and Cross Flow of 3D-Printed Rotational Mixing Vane in 2×3 Subchannel

Haneol Park

This certifies that the thesis of Haneol Park is approved.

07/09/2019

signature

_____

Advisor: In Cheol Bang

signature

_____

Chun Sang Yoo: Thesis Committee Member #1

signature

_____

Seung Jun Lee: Thesis Committee Member #2

Abstract

In pressurized water reactor (PWR), spacer grid is installed to support the fuel rod bundles, located between the fuel rod bundles. The mixing vane is installed on top of the spacer grid to generate swirl and cross flow. The swirl and cross flow enhance heat transfer and can promote critical heat flux of PWR. The safety margin of PWR could be estimated with heat transfer performance and CHF. So, the swirl and cross flow generation could bring about the safety margin and power uprate enhancement.

3D-printing technology enables to produce exquisite mixing vane blade component. The part of mixing vane was built by 3D printing. The general material is gypsum, the other is metal, stainless steel. The mixing vane is attached on top of the spacer grid, which also made by 3D printing.

Rotational mixing vane is a swirl generator between the fuel rod, improve the cross flow and heat transfer characteristics. Centrifugal force provides bubble detachment from the fuel rod surface.
Various types of rotational mixing vanes (RV) are studied. They are : the fan vane (FV), impeller vane (IV), the wind turbine vane (WT). Each RV shows different mixing performance and pressure drop. The FV shows the average mixing performance and pressure drop increase. The IV shows the most mixing performance, and the WT shows the least pressure drop.

Experimental approach, the Particle Image Velocimetry (PIV) experiment technique visualizes flow field and evaluates mixing performance. Flow pattern visualization is accomplished inside the 2×3 subchannel, 2.5 times scale-up test section. Tests shows the flow pattern tracking and measures pressure drop. The test assures durability and maintainability of 3D printed mixing vane parts equipped in the subchannel.

Numerical analysis is conducted using the commercial using computational fluid dynamics (CFD) code FLOW-3D. General Moving Object (GMO) method is used to simulate flow-driven coupled rotational motion. The Fluid-structure interaction (FSI) problem is too complex to solve analytically, so the computational technique to validate the rotational motion is also researched. The mixing performance of rotational mixing vane is evaluated by swirl and cross flow of coolant. The cross flow and swirl are

qualified the mixing performance as mixing parameters. The lateral velocity, vorticity, and bubble tracking method shows the mixing of coolant, as the mixing parameters. The pressure drop is also measured and friction factor evaluation is done to assure the system safety of the reactor.

For recommendation, further optimization of 3D printed mixing vane will be keep researched. Heat transfer characteristics and thermal performance enhancement for experimental and numerical analysis would be validated in extended subchannel. Adopting the rotational mixing vane in the PWR could results enhancement of the heat transfer performance, safety margin and power uprate.

Contents

Abstract …….. VI
Contents ……. . VIII
List of figures ...…….…… IX
List of tables ...……..... X
Nomenclature…….. XI

Chapter 1. INTRODUCTION

1.1 Rotational mixing vane in PWR (background) ……..... 1
1.2 Mixing performance parameters…….....2
1.3 Literature Survey…….... ... 3

Chapter 2. TEST PROCEDURE

2.1 Types of rotational mixing vane ……..... ... 8
2.2 Mixing vane experimental test section and manufacture procedures……..... 8
2.3 CFD Analysis Set-up (FLOW-3D) ……. . . . . ….. 10

Chapter 3. RESULTS AND DISCUSSION

3.1 Rotational motion description ……..... 21
3.2 Flow field at $Z/D_h = 1$ ……..... 22
3.3 Lateral velocity and vorticity ……... ... 23
3.4 Flow pattern tracking by bubble in 2×3 Subchannel ……... 24
3.5 Pressure drop evaluation ……..... 25

Chapter 4. CONCLUSION AND RECOMMENDATIONS

4.1 Conclusion…….....43
4.2 Recommendations ……..... .. 44

References……..... 47
Acknowledgement (감사의 글) ……..49

List of Figures

Figure. 1. 1 Mesh structure of rotational motion CFD simulation models

Figure. 2. 1 Geometry of mixing vane

Figure. 2. 2 Geometry of rotational mixing vane types

Figure. 2. 3 The Gypsum 3D printed rotational mixing vanes

Figure. 2. 4 Schematic diagram of mixing vane experiment facility

Figure. 2. 5 Mixing vane test section

Figure. 2. 6 (a) 2×3 subchannel test section for flow-driven rotational mixing vane in CFD

Figure. 2. 6 (b). 2×3 subchannel test section for flow-driven rotational mixing vane in CFD

Figure. 3. 1 Rotational speed evaluation

Figure. 3. 2 Lateral velocity flow field by PIV experiment

Figure. 3. 3 Lateral velocity flow field by PIV experiment, Z/Dh = 1, 2, and 3

Figure. 3. 4 Turbulent intensity by CFD analysis

Figure. 3. 5 2D-Flow field with lateral velocity vector (m/s)

Figure. 3. 6 2D vorticity field by CFD analysis

Figure. 3. 7 Lateral velocity distribution for mesh numbers, at Z/Dh = 1

Figure. 3. 8 Pressure drop for mesh numbers, at $Z/D_h = 1$

Figure. 3. 9 lateral velocity comparison at $Z/D_h = 1, 2, 3$

Figure. 3. 10 Lateral velocity distribution, Q=145 lpm, Re=12,750, $Z/D_h = 1$

Figure. 3. 11 Bubble generation test in CFD analysis, Q=145 lpm

Figure. 4. 1 3D printed metal mixing vane

Figure. 4. 2 3D printed mixing vane equipped spacer grid

List of Tables

Table. 1. 1 Previous research of experiment of subchannel with mixing vane

Table. 2. 1 CFD boundary condition

Table. 3. 1 The area average lateral velocity for each mixing vane type

Table. 3. 2 The area average vorticity for each mixing vane type

Table. 3. 3 The pressure drop evaluation for experiment test section

Table. 3. 4 The pressure drop evaluation for CFD analysis using FLOW-3D

Nomenclature

	Roman Letters	
$\vec{u}$	velocity of object	[m/s]
F	force	[N]
m	total mass of object	[kg]
T	total torque	[N]
$[J]$	inertia tensor	
V_f	volume fraction	
A	area fraction	
S_{obj}	area of object	[m/s]
S_m	physical mass source term of fluid	[kg/m^3]
Q	Flow rate	[liter/min]
r	distance from G to P	

	Greek Letters	
$\vec{\omega}$	angular velocity	[rad/s]
$\vec{u}$	velocity of object	[m/s]
ρ	density	[kg/m^3]
ζ	Vorticity	[1/s]

	Subscripts
P	*Point of object*
G	*Mass center of object*
M	*Mass source of fluid*
obj	*Object*
f	*Fraction*
cell	M*esh cell*

Abbreviations and acronyms

BG	Bare Grid (spacer grid without vane)
RV	Rotational Vane
SV	(Fixed) Split Vane
FV	(Rotational) Fan Vane
IV	(Rotational) Impeller Vane
WT	(Rotational) Wind Turbine Vane
CFD	Computational Fluid Dynamics
PIV	Particle Image Velocimetry

Chapter 1. INTRODUCTION

1.1 Rotational Mixing Vane in PWR

In Pressurized Water Reactor (PWR), fuel rod bundles are supported by spacer grid, located between the rod bundles. The mixing vane is installed on top of the spacer grid, to increase flow mixing. The mixing vane has role to promote mixing of the coolant (Critical heat flux and heat transfer enhancement), provide for axial expansion and growth of fuel rods, prevent flow-induced fretting wear, and prevent hang-up during fuel assembly loading/unloading. The benchmark study and hydrodynamic effect were studied widely. The thermal margin of PWR can be evaluated with heat transfer and CHF. So, focusing on the effect of mixing performance and CHF enhancement, the rotational mixing vane (RV) model was suggested. The fixed type mixing vane is presenting in the PWR, but flow mixing is limited to the specific location along with the shape of mixing vane. In addition, issue of pressure drop increase by typical fixed mixing vane is arising for PWR operator groups. For the improvement of swirl generation with reduced pressure drop in the subchannel, flow-driven RV was proposed. RV rotates with flow-driven rotational motion by Newton's third law, generates swirl in the subchannel with force toward the center. RV in single subchannel was suggested and its performance was evaluated first by Seo et al. In this research, fuel rod bundles were not included in the subchannel model. To examine the hydraulic characteristics of the whole rod bundle assembly of a real nuclear reactor, 2.5 times scaled up test section with RV was established.

The RV rotates with flow-driven rotational motion by flow induced force, not by artificial force. The flow-driven rotational motion equalizes cross flow and generates swirl with enhanced heat transfer performance and CHF enhancement. The lateral velocity and swirl decay were smaller than fixed split vane. The pressure drop is diminished comparing to fixed split vane. The cross flow and pressure drop was evaluated for various RV types, as shown in 2-1. The flow characteristic is evaluated as mixing performance of mixing vane.

1.2 Mixing performance parameters

The cross flow generated by the fixed split vane (FSV) and the swirl generated by the rotational vane (RV) was evaluated as mixing performance. 2×3 subchannel test section was made of acrylic material, to visualize the flow field by the PIV experiment and to observe rotational motion of RV. Therefore, isothermal condition experiment and analysis are conducted. For the isothermal condition, the lateral velocity of coolant developed by mixing vane.

First, velocity possesses value as mixing performance parameter itself. Cross flow of coolant can be shown as lateral velocity, divided by the bulk velocity average. The rotational speed for each RV was measured and validated for experiment and CFD analysis. Swirl and cross of mixing vane were evaluated with the velocity magnitude at the first stage.

Second, the vorticity evaluates the magnitude of centrifugal force. The swirl and vortices generated by flow-driven rotational mixing vane could be measured as vorticity, comparing the cross flow.

Vorticity is a pseudovector field that describes the local spinning motion of a continuum. Vorticity could be determined by marking parts of a continuum in a small neighborhood of the point of area, watching their relative displacements as they move along the flow. The vorticity vector would be twice the mean angular velocity vector of those particles relative to their center of mass, oriented according to the right-hand rule. This quantity must not be confused with the angular velocity of the particles relative to some other point. The vorticity is adopted as parameter for the centrifugal force evaluation.

$$\vec{\omega} \equiv \nabla \times \vec{u}$$

Third, flow pattern by bubble tracking method. PIV method tracks the single particle to measure the velocity, but it is hard to adopt to fluid dynamics. Instead to simulate the CHF, The air bubble visualized the flow pattern of coolant. Bubble behavior also visualize the velocity field. The flow pattern was shown as bubble behavior. Mechanistic approach of CHF enhancement could be studied with bubble behavior inside the mixing vane equipped subchannel.

Also, pressure drop issue inside PWR is arising for PWR operator groups, adopting the typical fixed mixing vane for the PWR. The rotational motion minimizes the blockage area of coolant comparing to the fixed mixing vane. So the pressure drop was measured for with mixing vane installed subchannel for fixed split vane, rotational fan vane, and fixed fan vane. Pressure drop could be evaluated as friction

factor, and DP/DP_0.

$$\text{friction factor} : f = \frac{2\Delta p d_h}{l \rho u_m^2}$$

$$\frac{\text{DP of mixingvane}}{\text{DP w/o mixingvane}} : DP/DP_0$$

In summary, the rotational speed was shown for the validation, lateral velocity and vorticity, as velocity field evaluation. The air bubble tracking method showed the flow pattern of coolant. Pressure drop evaluated the safety margin of PWR.

1.3 Literature Survey

The benchmark study and hydrodynamic effect were studied in [1] – [3]. The thermal margin of PWR can be evaluated with heat transfer and CHF. So, focusing on the effect of mixing performance and CHF enhancement, the roational mixing vane (RV) model was suggested. The fixed type mixing vane is presenting in the PWR, but flow mixing is limited to the specific location along with the shape of mixing vane. In addition, issue of pressure drop increase by typical fixed mixing vane is arising for PWR operator groups. For the improvement of flow mixing with reduced pressure drop in the subchannel, flow-driven RV was proposed by UNIST. A RV in single subchannel was suggested and its performance was evaluated [4]. In this research, fuel rod bundles were not included in the subchannel model. To examine the hydraulic characteristics of the whole rod bundle assembly of a real nuclear reactor, 2 x 3 subchannel with arcrylic fuel rod test section is designed.

To evaluate mixing performance of the innovative rotational mixing vane, particle image velocimetry (PIV) technique is utilized to visualize flow field and flow velocity in the test section, which is designed as 2.5 times scaled-up subchannel with 2x3 fuel rod bundles of typical PWR. Scaling is considered to maximize visualization and evaluate the mixing effect of mixing vane in fuel assembly subchannel [5] – [6]. The mixing performance, which can be represented by mixing parameters such as vorticity and swirl ratio, are compared with those of fixed mixing vane and bare grid. Also, computational fluid dynamics analysis methodologies were studied by CFD codes [7] – [9]. Numerical analysis with commercial computational fluid dynamics (CFD) code, FLOW-3D, is also conducted to reproduce test model of flow field obtained from PIV results. While typical split vane has highest peak cross flow in the subchannel, the RV concept has competitiveness and merit for equalized mixing by centrifugal force,

for lateral cross flow and swirl decay according to flow direction. Moreover, pressure drop test is conducted. The pressure drop due to grid spacer and mixing vane were studied [10] – [11]. The RV gives pressure drop decrease comparing to BG and SV. In short, RV effects on flow mixing and pressure drop are under study. The rotational motion of fan-generated swirl was studied [12]. Adopting the RV in the subchannel, the heat transfer performance and critical heat flux enhancement are expected, which will lead thermal margin improvement for the PWR.

The modeling of rotational motion in commercial CFD code focuses on RPM prescribed motion. The Moving Reference Frame(MRF), Sliding Mesh Model(SMM), and Dynamic Mesh Models(DMM) are general approaches. The MRF solved the equations in a rotational reference frame in terms of relative velocity. SMM uses non-conformal meshes between the rotational and fixed part of the domain. Usually to evaluate interface effect. DMM needs very fine meshes, useful to model relative motion between parts, but huge computational power is necessary.

To model the flow-driven motion was driven by newton's 3rd law without artificial force, advanced numerical analysis method was needed. Therefore, in the present study, the General Moving Object (GMO) method was applied. Commercial CFD code, FLOW-3D, was used. The General Moving Object (GMO) method was applied in FLOW-3D. The GMO method is unique technique in the FLOW-3D, by FlowScience Inc. (2009). In square lattice mesh, each solid and void fraction composed the rigid body and fluid. The hydraulic force was applied as driving force to the rotational motion of rigid body. Time variable rotational motion and its mixing effect to fluid were simulated by GMO method. Figure 1-1 shows the mesh models for rotational motions.

Moving Reference Frame

$$\frac{\partial}{\partial t}\left(\rho\vec{v}\right)+\nabla\cdot\left(\rho\vec{v}_r\vec{v}\right)+\rho(\omega\times\vec{v})=-\nabla p+\nabla\bar{\bar{\tau}}+\vec{F} \tag{1}$$

Sliding Mesh Model

$$\rho_F\left(\frac{\partial v_F}{\partial t}+(v_F\otimes\nabla)\cdot(v_F-v_F^m)\right)=\rho_F g+\nabla\cdot\sigma_F,\nabla\cdot v=0 \tag{2}$$

Dynamic Mesh Model

$$\frac{d}{dt}\int_V\rho\phi dV+\int_{\partial V}\rho\phi(\vec{u}-\vec{u}_g)\cdot d\vec{A}=\int_{\partial V}\Gamma\nabla\phi\cdot d\vec{A}+\int_V S_\phi dV \tag{3}$$

General Moving Object

$$-\frac{\partial V_f}{\partial t}=\frac{S_{obj}}{V_{cell}}\vec{V}_{obj}\bullet\vec{n} \tag{4}$$

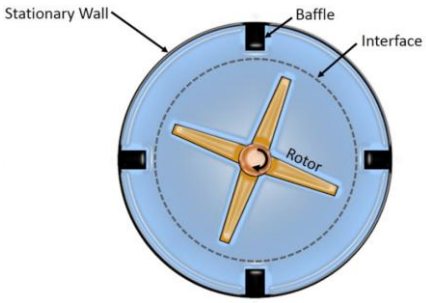

(a) Moving Reference Frame

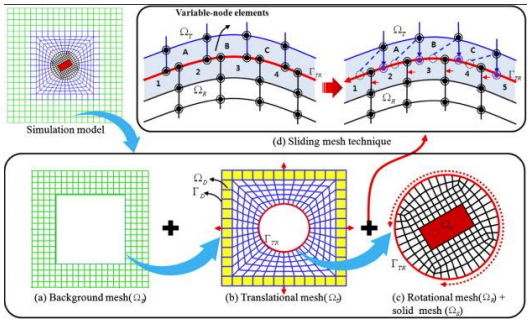

(b) Sliding Mesh Model

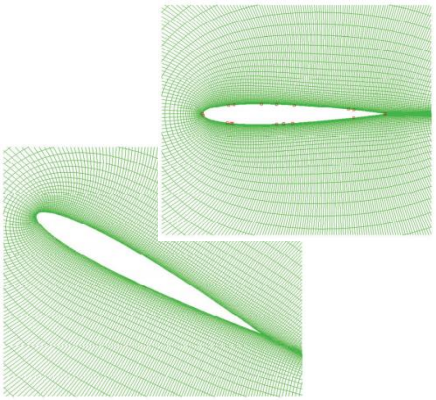

(c) Dynamic Mesh Model

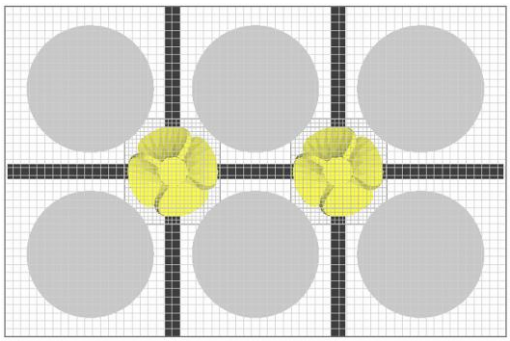

(d) General Moving Object

Figure. 1. 1 Mesh structure of rotational motion CFD simulation models

Table. 1. 1 Previous research of experiment of subchannel with mixing vane

	McClusky et al. (2003)	Podila et al. (2014)	Lee et al. (2007)	Yang et al. (2017)	Seo et al. (2015)	Present research (UNIST)
Subchannel	5x5	5x5	8x8	5x5	single	2x3 (6 fuel rod)
Mixing vane	Split pair vane	Split vane	Small scale vortex flow, large scale vortex flow (SSVF & LSVF) mixing vane	Split mixing vane, Separate mixing vane	Rotational Mixing vane	Rotational mixing vane: Fan, Impeller, Wind turbine
Procedures	LDV, CFD	CFD (ANSYS)	CFD (FLUENT)	CFD (ANSYS CFX)	PIV, bubble injection, CFD (FLOW-3D)	PIV, ΔP, CFD (FLOW-3D)
Parameters	Velocity ratio, Lateral kinetic energy	Velocity (Spanwise, transverse, axial), Vorticity, URMS/W	Flow intensity, Pressure drop	Synergy angle, Pressure loss, Nu	Velocity, Swirl ratio, bubble behavior	Velocity, Vorticity, Pressure drop, bubble behavior

Chapter 2. TEST PROCEDURES

2.1 Types of rotational mixing vane

Figure 1. shows the geometry of spacer grid attached to the test section and the mixing vane installed on top of the grid. Bare grid (BG), and fixed split vane (SV) designed based on the spacer grid structure. The spacer grid is a wall with 3 mm thick, 100 mm length, and 66 mm width. The fixed split mixing vane for KSNP was used. The rotational mixing vane (RV) is equipped on top of the BG.

Figure 2. Shows the rotational mixing vane types with different vane blades. All rotational vanes were designed with same length and height of blade. The RV model has four blades, same angle with SV. Length of blade is 6 mm with height is also 6 mm, and thickness is 0.6 mm for the vane blades. A hole is drilled at the center of the rotational vane to attach vane to the spacer grid. Fan Vane (FV) design was selected for the basic model of RV as Korean patent [13]. Impeller Vane (IV) was designed with 16 vane blades, which will maximize the mixing effect. The angle of blade was 45° also. Keep the angle same, the blade number and area were maximized to mixing. Wind turbine Vane (WT), was designed as N-10 air turbine structure, by Air foil plotter. Vane length was 6 mm and vane width was 6 mm. The pressure drop and flow blockage is minimized with WT. The application of optimized vane design might be differ by the purpose and performance of the vanes.

2.2 Mixing vane experimental test section and manufacture procedures

Fig. 1-3 shows a schematic diagram of experimental facility and mixing vane test section. Major components of the facility include water tank, pump, flow meter, dP transmeter, PIV laser, CCD camera, data acquisition system and the mixing vane test section.

The mixing vane was placed in the test section, simulating the subchannel with fuel rod assembly and mixing vane equipped spacer grid. Test section is designed with rectangular subchannel, with 2×3 fuel rod. Test section was 2.5 times scaled-up comparing to the typical Plus-7 fuel assembly channel. The scaling was considered to maximize visualization and evaluate the swirling effect of mixing vane in fuel assembly subchannel. As subchannel test section, Acrylic channel with thickness of 10 mm was

used. The 2×3 subchannel had 99 mm length, 66 mm width and the total height is 300 mm. The test section is composite with 3 part of 100 mm duct each. The ducts each have pressure tap, air injection tap, and grid flange. They could be assembled any order, to retain various Z/D_h. By assembling different order, PIV, pressure drop, air bubble injection test could be done with single test section.

Pin pitch was 33 mm. The acrylic fuel tube with the diameter of 25.4 mm was installed from the top-to-bottom of test section, fixed by grid flange. For the PIV measurement, extended acrylic fuel tube was attached to the top of the fuel rod. The subchannel was also made of acrylic to penetrate PIV laser and visualize the section.

Adopt baring between spacer grid and RV to minimize friction. The spacer grid and mixing vanes were fixed to the test section. The BG, SV, and RV equipped spacer grid were attached to the test section Attached to the hole by 2t bolt. 6 edges of spacer grid attached to the test section with acrylic flanges.

The spacer grid and mixing vane on top of the spacer grid were installed at the middle side of the test section. Acrylic ducts fixed each side of spacer grid. It was designed to make the BG, SV, RV can be replaced for each test. The inlet and outlet were 4-way split line to the test section from each side. They helped straighten vertical flow. Also, the mirror could be installed on top of the test section, to visualize horizontal flow field. The flow direction in the test section was vertical against the gravity.

For the PIV experiment, silver-coated hollow glass spheres, were selected as a seeding particle. The mean diameter was 20m, density was 0.1g/cc, same with the working fluid. Water with 1 bar at room temperature was used as working fluid.

A differential pressure (dP) gauge was located in the test section to measure the pressure drop. To measure dP, pressure tap positions at the upper and lower part of the test section. Each pressure tap was connected to pressure transmitter calibrated with 0.005kPa accuracy. The pressure drop at the spacer grid and mixing vane was evaluated by the pressure difference at upstream and downstream from the spacer grid.

The durability and maintainability were tested with 3D printed parts. The 3D printed RV and its

attachment were tested inside the test section. With the fluid flow, rotational motion and attachment were experimentally tested during the test period.

2.3 CFD Analysis Set-up (FLOW-3D)

The mesh type in FLOW-3D was hexahedral mesh. Fractional Area/Volume Obstacle Representation (FAVOR) mesh system was applied in FLOW-3D. Unique FAVOR technique describes complex geometry in Volume of Fluid (VOF) model. The Volume of Fluid (VOF) is based on the idea of recording in each grid cell the fractional portion of the cell volume is occupied by liquid.

In FLOW-3D, free surfaces are modeled with the VOF technique, which was reported in Nichols and Hirt (1975). The VOF method consists of three ingredients: a scheme to locate the surface, an algorithm to track the surface as a sharp interface moving through a computational grid, and a means of applying boundary conditions at the surface.

The VOF concept is crucial when solving GMO problem. The fraction of solid and fluid is calculated in hexahedral mesh. Where the fraction is between 0 to 1 is assumed as the surface. The hydraulic force applied as source term to the solid motion. The solid motion is calculated as 6-degrees of freedom motion – 3 transportation and 3 rotational motions, or motion constraints such as a fixed axis/point. It could have both prescribed or dynamically coupled with fluid flow.

The Fractional Area/Volume (FAVOR^{TM}) method is adopted is adopted to simply model the complex geometric regions. The FAVOR™ concept can be used in connection with any type of grid including grids consisting of rectangular or distorted elements and whether the grid is structured or unstructured. Structured grids are best because they are easy to generate and the indices for neighboring elements are known. Rectangular grid elements make it easy to compute the fractional areas and volumes of elements used by the FAVOR™ method.

The fluid and geometry regions were computed by the open area fraction on the cell faces along with the open volume faction and reconstructs the geometry based on these parameters. That represent complex surfaces in the domain without requiring a body-fitted grid. The mesh structure was generally consisted of uniform hexahedral structure. However, multi-block mesh technique was applied to simulate accurate motion of vanes. The mesh blocks were divided into two types: uniform mesh and vane mesh. The internal block cell size for specific area was 2.0. So uniform mesh with 1.0 mm mesh size for the fluid region, and vane mesh with 0.5 mm mesh size for the vane region were applied.

Table. 2-1 shows the boundary condition for the CFD analysis model. Two-equation (k-w) model was adopted for the turbulence flow. Implicit, GMRES solver was used for pressure. The subspace size was 15, inter-block boundary type coefficient was set as 0.25. The flow speed was the same as the experimental condition, 0.7 m/s. The initial and inlet fluid velocity was set as 0.7 m/s, relative outlet pressure was set as 0 Pa. The air-bubble injection was also conducted. Particles were generated at the 8 position near the fuel rod. 3200 particles were generated, following the axial position as 0 mm – 120 mm from the bottom of the test section.

2.3.1 Governing equation General Moving Object method

The GMO model can be described as follows :

Rigid body rotates about fixed axis, non-inertial force and torque

$$\vec{\boldsymbol{V}}_P = \vec{\boldsymbol{V}}_G + \vec{\omega} \times \boldsymbol{r}_{P/G} \tag{1}$$

Denoting P as a point on the object, its velocity is related to the mass center velocity V_G, r and angular velocity ω, from the distance r of the rigid body.

The first term on the right-hand side of equation (6) represents translation of the mass center and the second term is the rotation about the mass center. Note that ω r is a property of the moving object and is independent of the choice of the base point. Equations of motion governing the two separate motions are

$$\vec{F} = m\frac{d\vec{V}_G}{dt} \tag{2}$$

$$\vec{T}_G = [J]\cdot\frac{d\vec{\omega}}{dt} + \vec{\omega}\times\left([J]\cdot\vec{\omega}\right) \tag{3}$$

where F is the total force, m is the rigid body mass, T_G is the total torque about G, [J] is moment of inertia tensor about G in the body system (inertia tensor).

The general form of the continuity equation based on the FAVOR™ method is

$$\frac{\partial}{\partial t}(\rho \boldsymbol{V}_f) + \nabla \bullet (\rho u A) = S_m \qquad (4)$$

where S_m is a physical mass source term of fluid, Vf and A are volume and area fractions. In contrast to stationary object problems, V_f and A vary with time in moving object problems and their effects on fluid flow must be considered. Equation (1) can be rewritten as

$$\frac{V_f}{\rho}\frac{\partial \rho}{\partial t} + \frac{1}{\rho}\nabla \bullet (\rho u A) = -\frac{\partial V_f}{\partial t} + \frac{S_m}{\rho} \qquad (5)$$

For incompressible flow, it is reduced to

$$\nabla \bullet (\vec{u} A) = -\frac{\partial V_f}{\partial t} + \frac{S_m}{\rho} \qquad (6)$$

Comparing with the continuity equation for stationary object problems, $-\frac{\partial V_f}{\partial t}$ is equivalent to an additional volume source term. When using the finite volume method, this source term exists only in mesh cells around moving object boundaries. For a first-order approximation in time, $-\frac{\partial V_f}{\partial t}$ can be discretized into

$$-\frac{\partial V_f}{\partial t} = -\frac{{V_f}^n - {V_f}^{n-1}}{\delta t} \qquad (7)$$

where the upper indices n-1 and n denote the variable values at the previous and current time steps, respectively, and t δ is the time difference.

For the general moving object, mass conservation equation is rewritten into

$$-\frac{\partial V_f}{\partial t} = \frac{S_{obj}}{V_{cell}} \vec{V}_{obj} \bullet \vec{n} \qquad (8)$$

V_{cell} is the total volume of the mesh cell, S_{obj} , n and V_{obj} are the area, unit normal vector and velocity of moving object boundary in the mesh cell, respectively for object's shape and motion.

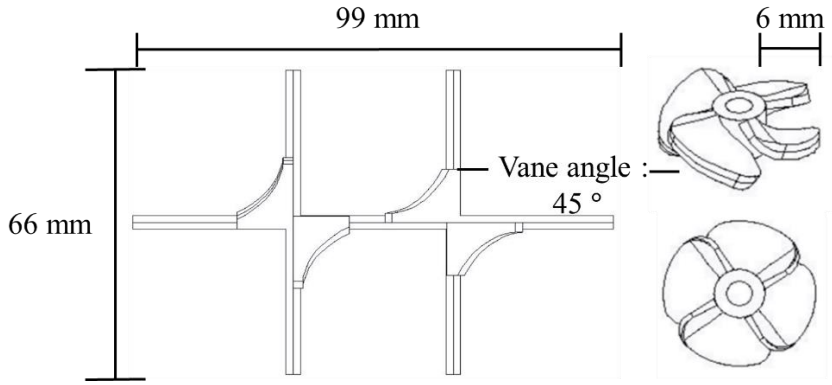

(a) Bare Grid (BG) and Fixed Split Vane (SV) (b) Rotational Vane (RV)

Figure. 2. 1 Geometry of mixing vane

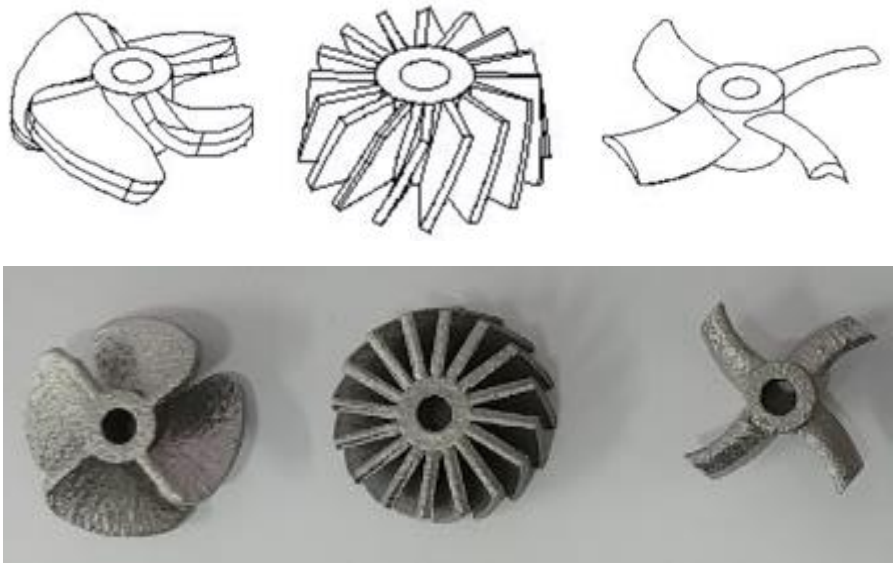

(a) Fan Vane (FV) (b) Impeller Vane (IV) (c) Wind Turbine Vane (WT)

Figure. 2.2 Geometry of rotational mixing vane types

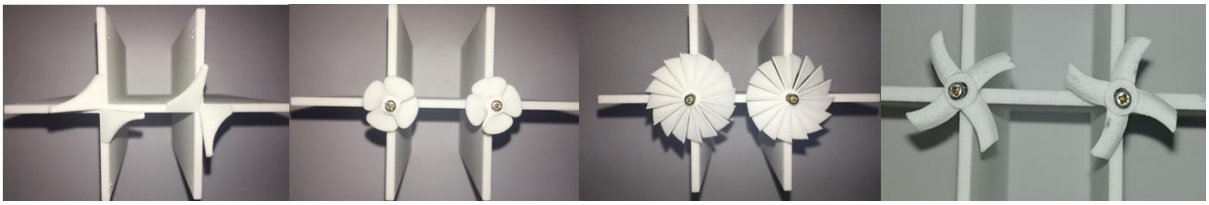

(a) (b) (c) (d)

Figure. 2.3 The Gypsum 3D printed rotational mixing vanes
(a) Fixed Split Vane (FSV) (b) Rotational Fan Vane (RFV)
(c) Rotational Impeller Vane (RIV) (d) Rotational Wind Turbine vane (RWT)

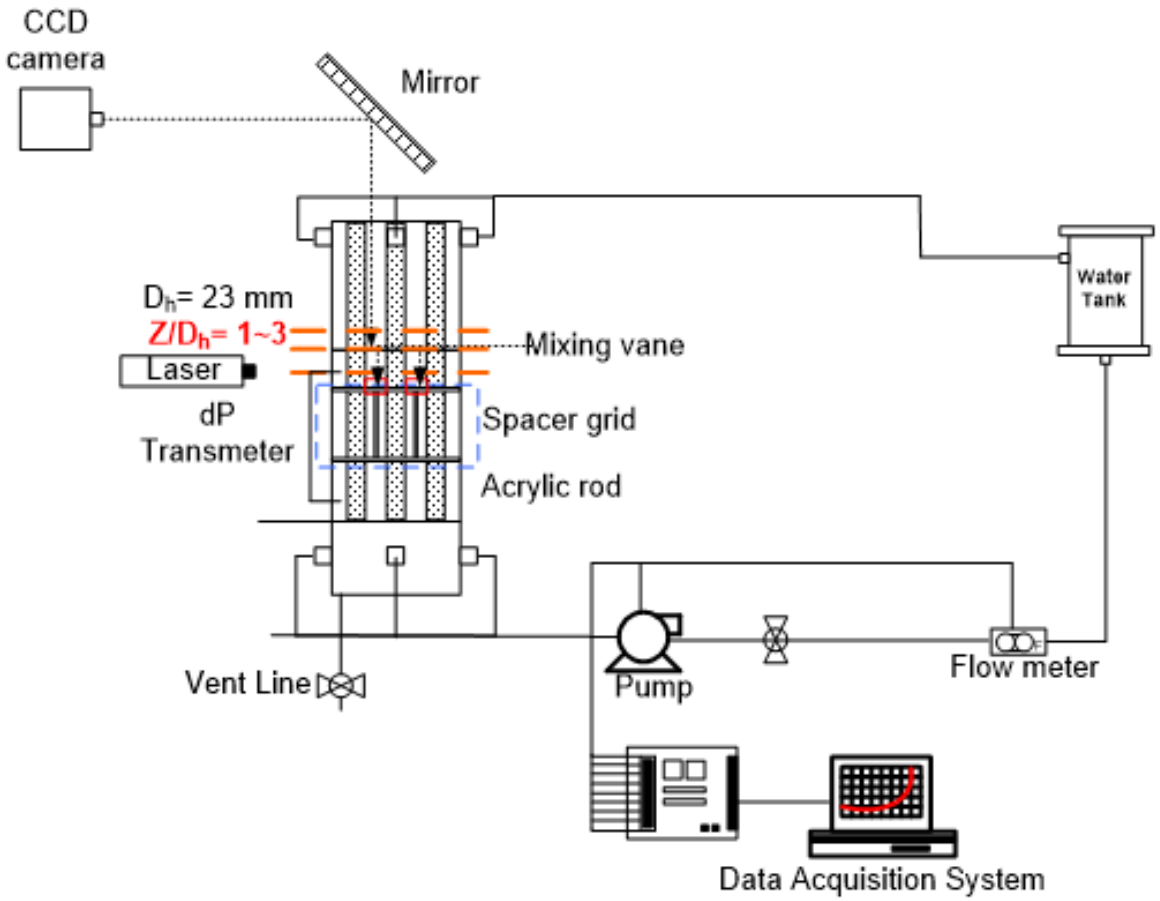

Figure. 2. 4 Schematic diagram of mixing vane experiment facility

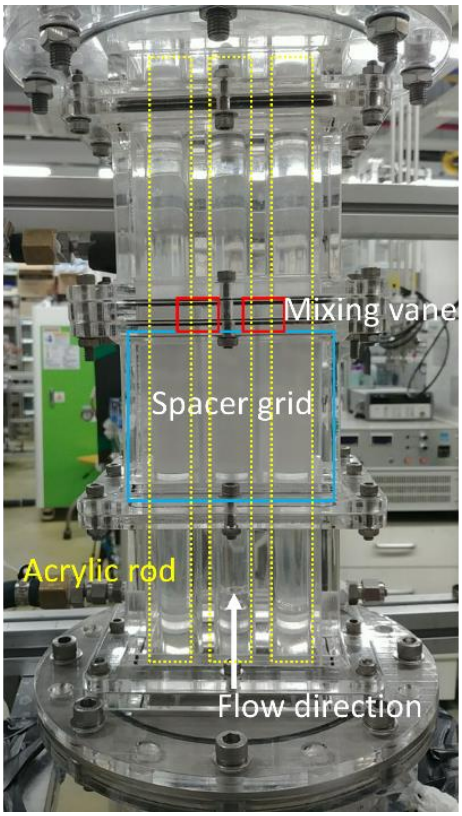

Figure 2. 5 Mixing vane test section

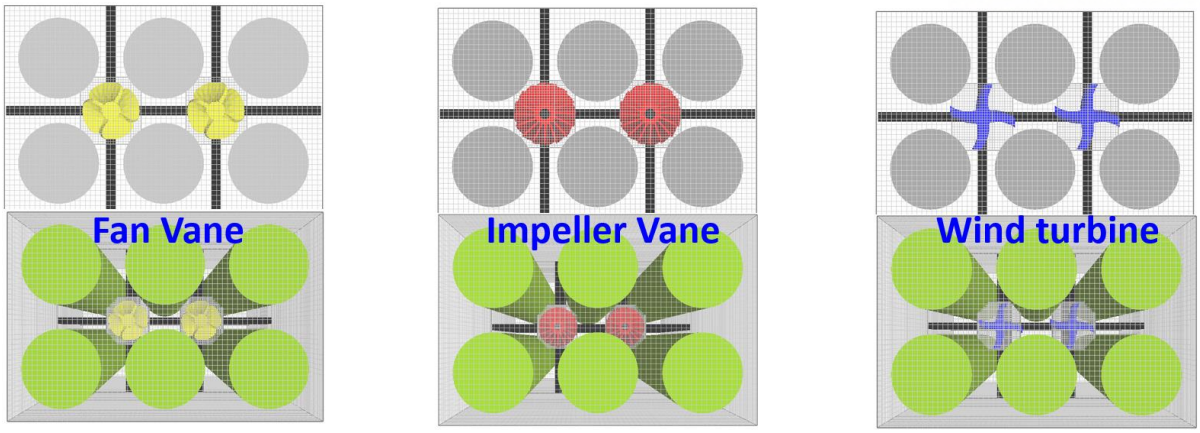

Figure. 2. 6 (a) 2×3 subchannel test section for flow-driven rotational mixing vane in CFD

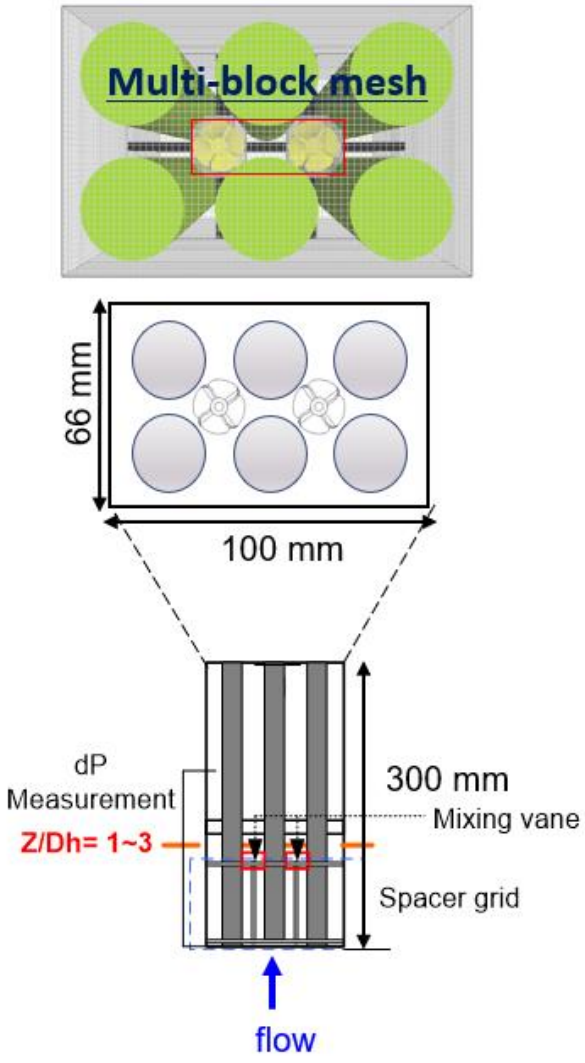

Figure 2. 6 (b). 2×3 subchannel test section for flow-driven rotational mixing vane in CFD

Table. 2. 1 CFD boundary condition

Parameter	**Value**
CFD tool	**FLOW-3D**
Axial velocity	0.7 m/s (Q = 145 lpm, 680 kg/m^2 s)
Mixing vane types	Fixed split vane(FSV) Rotational fan vane (RFV), Impeller vane (RIV), Wind turbine vane (RWT)
Rotational Motion	General Moving Objective (GMO)
Mesh type	Uniform mesh + Multi-block mesh
Turbulence model	RNG k-ω model

Chapter 3. RESULTS AND DISCUSSION

3.1 Rotational motion description

The flow-driven rotational motion of high speed camera experiment and GMO method computational analysis was validated.

Figure. 3. 1 shows the motion of rotating mixing vane in the 2×3 subchannel. The high speed camera experiment measures as 10 FPS, and computational analysis shows rotational motion as 16 FPS. The rotation speed of the fan vane was 1200 RPM by the high speed camera experiment, as fig. 3-1 (a). The rotation speed by the GMO was 950 RPM, respectively. The angular velocity was obtained by the simulation results, with visualized as fig. 3-1 (b). The experiment and the simulation results showed 20.83% difference. It is due to the difference of material property. The FV was made of gypsum. In contrast, the material property for the GMO was fixed as default, stainless steel. The density difference was estimated to bring the different rotation speed. As the friction between the solid and fluid were set as negligible in CFD analysis, the output rotation speed could even faster if the applied material properties. The friction coefficient of solid and fluid were set as 0, so the rotational motion were underestimated. But comparing to the artificial force with RPM input, GMO is valuable with estimating the flow-driven rotational motion. The prescribed rotational motion and flow-driven rotational motion were simulated with FLOW-3D.

The rotational speed of the IV and WT were also obtained, it was 669 RPM for IV, and 967 RPM for WT. The total mass of subcomponent of solid part affected to the rotational motion. The prescribed motion with obtained RPM were used as the mixing performance evaluation for later chapters. Flow-driven coupled motion and prescribed rotational motion are physically different by the Fluid-Structure Interaction (FSI) concept.

The durability and maintainability of RV were also validated by the rotational motion in the test section. The attachment and rotational motion of RV were maintained for 168 hours. The fixed screw and the 3D printed mixing vane itself both were durable in the test period. Admittedly, the test condition was much moderate than that of real PWR in high temperature and high radioactive condition. Also the test period were much shorter than real part of PWR in the PWR. Nevertheless, this test could be the first stage of check the manufacturability and the durability of 3D printed part adopting in the reactor with fluid flow condition.

3.2 Flow field visualization

The visualization of 2D velocity field at lateral cross section were done. Figure 3-2 to 3-6 show the 2D flow field.

Figure 3. 2 showed the cross flow and swirl at $Z/D_h = 1$. The lateral velocity field was measured the flow pattern of coolant, the cross flow and swirl shape. The FSV indicated the cross flow along with the mixing vane. The cross flow offset was occurred. This cross flow offset could increase the mixing between subchannel. Cross flow offset helps to reduce the maximum temperature of specific point. However, hot spot could exist following the cross flow, the heat transfer performance and bubble at the CHF condition could diverge with the cross flow. In contrast, the RFV showed the equalized cross flow with swirl generation. The mixing between subchannel was not developed due to the same direction of swirl. Instead, the equalized cross flow and centrifugal force of swirl could enhance the heat transfer from the fuel rod to the coolant. The cross flow offset would be made up to the swirl direction. But vorticity and pressure drop effect was focused for the rotational mixing vane.

Figure. 3. 3 shows the flow fields and lateral velocity of BG, SV, and RV, from $Z/D_h = 1$, 2, and 3. BG showed little lateral velocity. FSV showed more velocity, showing drastic decay following to the downstream of 2×3 subchannel. The RFV showed equalized cross flow, and small swirl field were generated at the center of the subchannel. The swirl and cross flow both developed to the downstream of the 2×3 subchannel. The magnitude of lateral velocity up to Z/D_h would be studied at chapter 3.3.

The maximum lateral velocity was respectively high in SV, the decay of lateral velocity was high along with the z-axis development. The swirl decay is measured by the lateral velocity driven through the z-axis. Comparison to Z/Dh = 1, lateral velocity loss is represented as decay. The decay effect was generated for both FSV and RFV, but distinguished swirl decay difference were not measured. The swirl and cross flow should be studied focusing on the Z/Dh = 1, to maximize the mixing performance. The swirl and cross flow decay were visualized with turbulent intensity. The mixing performances of both FSV and RFV were reduced to the downstream of the flow.

Fig. 3. 4 shows the flow fields and lateral velocity for CFD analysis, at the $Z/D_h = 1$. The turbulent intensity field was shown for the CFD analysis. The turbulent intensity shows the swirl decay through axial direction for the downstream of the 2×3 subchannel. The decay for FSV and RFV, and RIV were indicated as turbulent intensity. From the center of the 2×3 subchannel, the maximum turbulent intensity and velocity was observed, the flow decays to the outer direction toward the fuel rod. Due to the swirl decay, PIV experiment and CFD analysis for 2.5 scaled up subchannel for $Z/D_h = 1$ would be

considered to show the mixing effect.

Figure. 3. 5 shows the 2D velocity field at the $Z/D_h = 1$ by CFD analysis. The CFD analysis results emphasized view of the center of the subchannel. The mixing performance of SV and RV were evaluated with the velocity magnitudes and directions. The magnitude of velocity was bigger in SV, respectively. As shown in Fig. 3. 5 (a), SV showed flow along with the vane. The cross flow formed with x-axis and y-axis direction for each vane structure. In Fig. 3. 5 (b), RV blended with counter-clockwise direction swirl. The shape of swirl is almost steady regardless of time, because rotation speed was fast enough to equalize the flow. RV formed swirl at the center of the subchannel, which would concentrate the bubbles. These mixing characteristics would bring CHF enhancement when heated condition.

Centrifugal force could bring about CHF enhancement. Measurement of centrifugal force and swirl were studied by the vorticity parameter.

Figure. 3. 6 shows the vorticity at the $Z/D_h = 1$ by CFD analysis. Vorticity is a pseudo vector field that describes the local spinning motion of a continuum. The sign of vorticity represents the direction of swirl. + sign indicates the counter-clockwise direction swirl. – sign indicates the clockwise direction swirl. It is due to the rotation of earth is signed as positive value.

The Figure. 3. 6 (a) showed the comparison between the FSV and RV types, and 3. 6 (b) showed fixed concept of FV, IV, and WT. The swirl direction is reversed for rotational and fixed mixing vane. The swirl and centrifugal force was more affected by the rotational motion than the shape itself. There could be various hydraulic parameter that affects to swirl and vorticity magnitude. More optimization for shape and rotational direction of RV would be studied for further work.

3.3 Lateral velocity and vorticity magnitude

First, mesh convergence test was done to validate the CFD analysis with experimental results. Mesh numbers from 300k to 1500k were tested. Also, uniform mesh and multi-block mesh were tested. Multi-block mesh was set at the mixing vane area, to simulate accurate geometry and motion of mixing vane. The velocity and pressure convergence were tested for CFD analysis mesh. 300k mesh showed difference lateral velocity and pressure for the center of the section.

Figure 3-7 showed the lateral velocity distribution, and figure 3-8 showed the pressure drop for the test

section. The swirl decay to the axial position was bigger in FSV than FRV. When comparing the magnitude of the velocity, CFD under-estimated the results. These results were keep reported by the previous research for FSV and subchannel. The uncertainty for the fuel rod surface and the perplexity of the subchannel made hard to predict turbulence of the fluid. Yet more CFD analysis should be validated for both subchannel, and the rotational motion of flow-driven RV concept.

Table 3-1 showed the area-averaged lateral velocity, and table 3-2 showed the area-averaged vorticity for the subchannel. The RIV showed most mixing performance lateral velocity and vorticity. The FSV showed same lateral velocity with RIV only with 0.003 m/s difference, but the vorticity showed 15 (1/s) difference with bigger centrifugal force for the RIV.

Figure 3. 10 shows lateral velocity field at axial position of Z/Dh = 1 from the vane edge. FSV shows drastic mixing effect beside the fuel rod. FSV shows high lateral swirl but swirling area is highly dependent on the vane region. RFV and RIV generates swirl flow for lateral velocity, comparing to FSV has relatively small but swirling is occurring evenly along with large area of subchannel. RWT showed the least lateral velocity and vorticity even with more equalized-bigger shape of swirl.

Figure 3. 10 shows the lateral velocity distribution in subchannel in 2×3 subchannel.

3.4 Flow pattern tracking by bubble in 2×3 Subchannel

Figure. 3-9. Shows bubble injection test in CFD. Particle tracking method was applied by using gas particles, compared to the working fluid. The motions of bubbles were indicated as particles. The color of particle implies the axial position of particle. Blue and green particles were bubbles before pass the mixing vane, meanwhile yellow and red bubbles were downstream of the mixing vane. The upper view and the side view were shown.

The bubble was straight in BG. As seen in Figure 3-9. (a), the FSV model shows the motion of bubble due to cross flow. The bubbles followed specific pass through the angle of mixing vane. The bubble flowed with the mixing between the subchannel. Figure. 3-9 (b) to 3-9 (d) shows the air bubble injection results for the RV model. For the RV model, bubbles were gathered at the center position of subchannel. The bubbles were evenly distributed to the center of the subchannel. Bubble particles touched against the mixing vane with different angle as the time-dependent position of mixing vane. The time-dependent position of mixing vane was differs time by time as flow-driven rotational motion. Also the rotational motion generate centrifugal force with swirl flow. Due to the centrifugal force, fluid near the fuel surface

would be transferred depart from the fuel rods. Therefore, the CHF could be enhanced by the air bubble detachment from the fuel rods.

As seen in Fig 3-9. (a), the FSV model shows the diverging pattern. The bubbles followed specific pass through the angle of mixing vane. The bubble move through the subchannel. Figure 3-9. (b), (c) and (d) shows the air bubble injection results for the FV model. For the FV model, bubbles were gathered at the center position of subchannel. The bubbles were evenly distributed to the center of the subchannel. As with the previous results for flow field and lateral velocity, IV showed the most mixing and the bubbles were equalized most. The FV also showed well converging pattern to the center of the subchannel. The WT showed converging effect but due to small cross flow, the effect was smaller. The time-dependent position of mixing vane was differs time by time as flow-driven rotational motion. Also the rotational motion generate centrifugal force with swirl flow. Due to the centrifugal force, fluid near the fuel surface would be transferred depart from the fuel rods. Therefore, the CHF could be enhanced by the air bubble detachment and the reduced void fraction near the fuel rods.

3.5 Pressure drop evaluation

Table 1. lists the pressure drop measurement results obtained from the experiment. The pressure drop of BG (dP_0) was 0.41 kPa for the Q = 145 lpm, v = 0.7 m/s and Re = 12,500. The P/P_0 was increased in FSV, as dP/dP_0 = 1.037, respectively. The friction between fluid and fixed vane caused the largest pressure drop. In contrast, RV mitigated pressure loss with comparatively in experiment by the dP/dP_0 = 1. The pressure drop was lower for RV than SV, because blockage of the flow was decreased with the motion of the rotational vane. Therefore, RV could be additionally installed without concerning the pressure drop of the reactor. For the CFD results, BG showed 0.206 kPa respectively, dP/dP_0 were reduced as 1.025 and 1.018 for FSV and RFV. The RIV and RWT also studied, with showing the dP/dP_0 = 1.004 and 0.96.

The friction factor was evaluated much smaller than previous pressure drop research. The friction effect of grid and wall of test section is reduced. So the pressure drop evaluation was underestimated for both experiment and CFD results. However, the RV types showed less pressure drop than FSV and FFV. RFV, RIV, RWT showed the reduced pressure drop than FSV case in BG. Because blockage of the flow was decreased with the motion of the rotational vane. Therefore, RV could be additionally installed without concerning the pressure drop of the reactor.

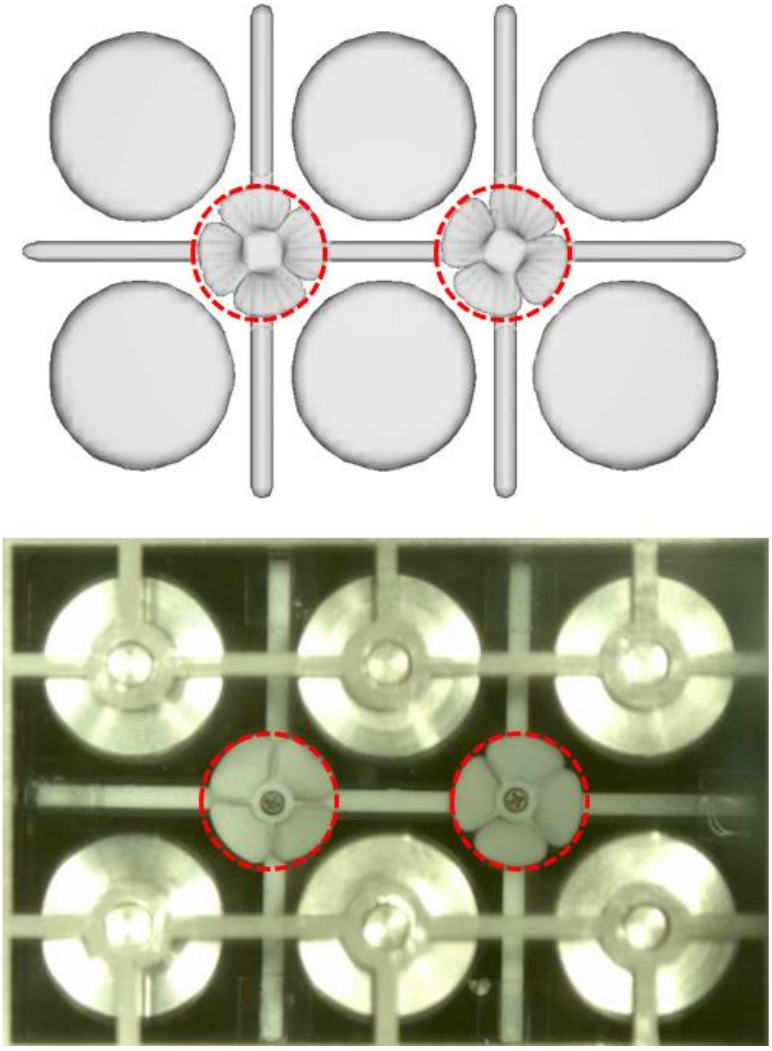

Figure. 3. 1 Rotational speed evaluation
(a) from GMO model of FLOW-3D (10 FPS) (b) from high speed camera experiment (16 FPS)

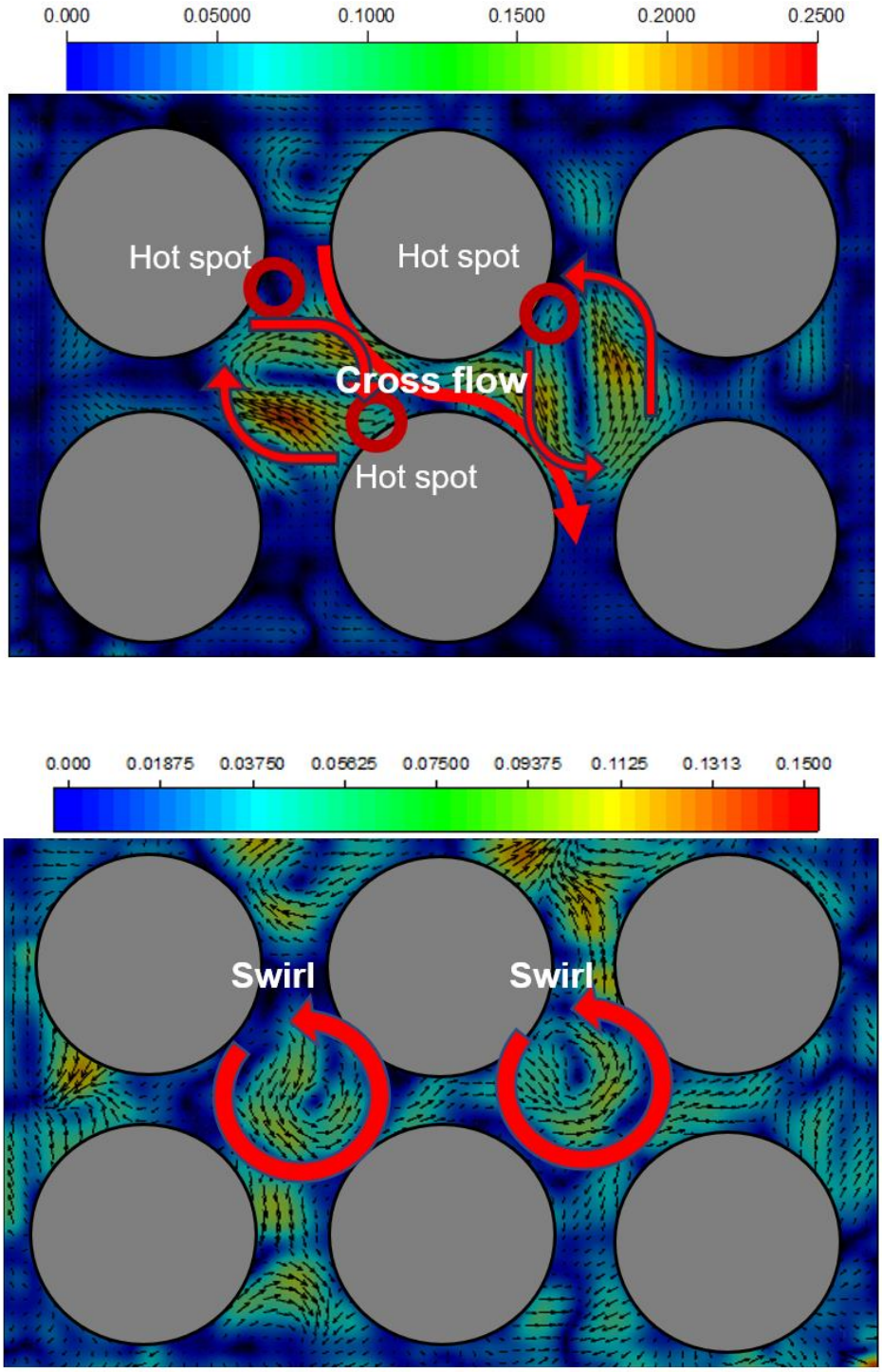

Figure 3. 2 Lateral velocity flow field by PIV experiment (Q=145 lpm, v=0.7 m/s, Re=12,750)

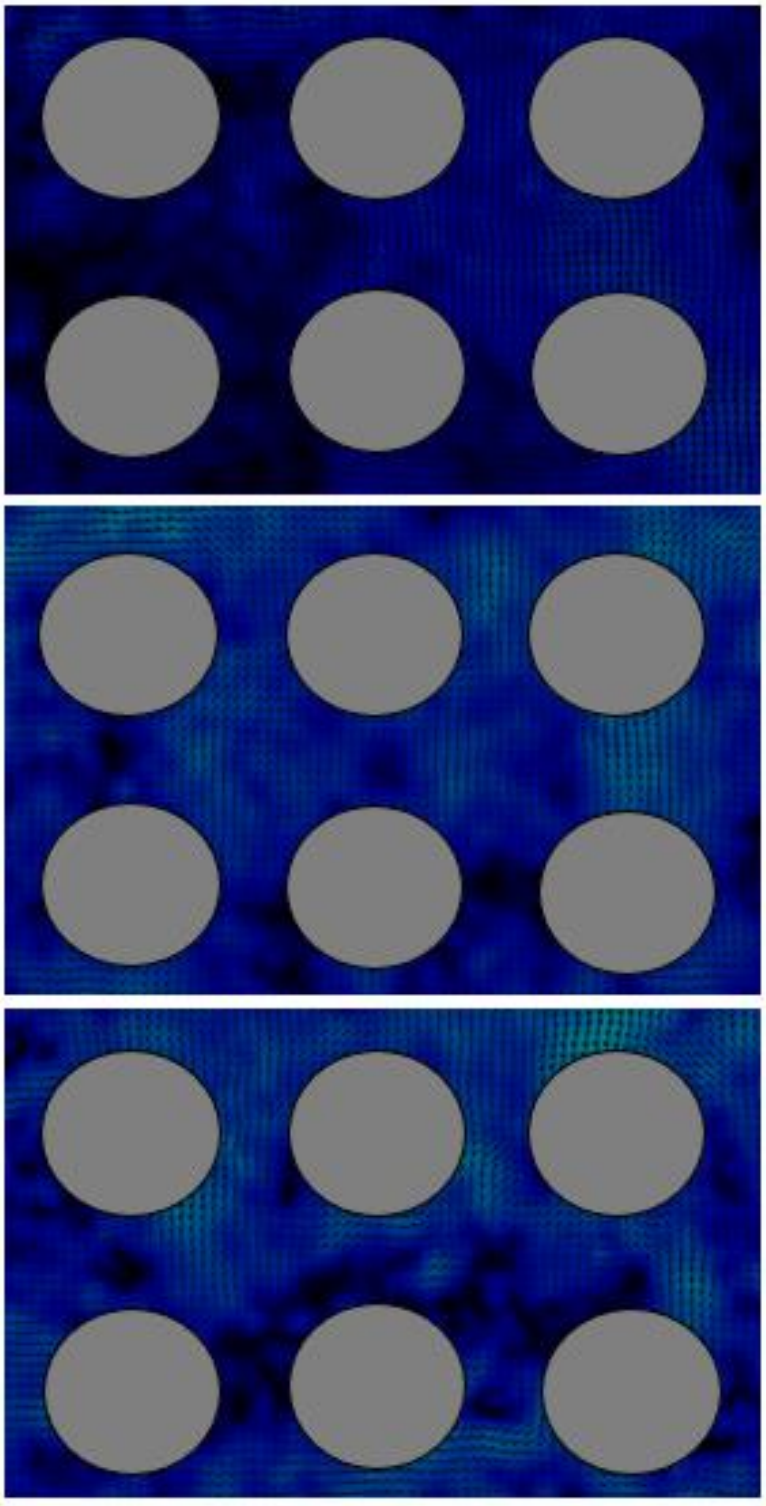

Figure. 3. 3 (a) Lateral velocity flow field by PIV experiment, Z/Dh = 1, 2, and 3 for BG

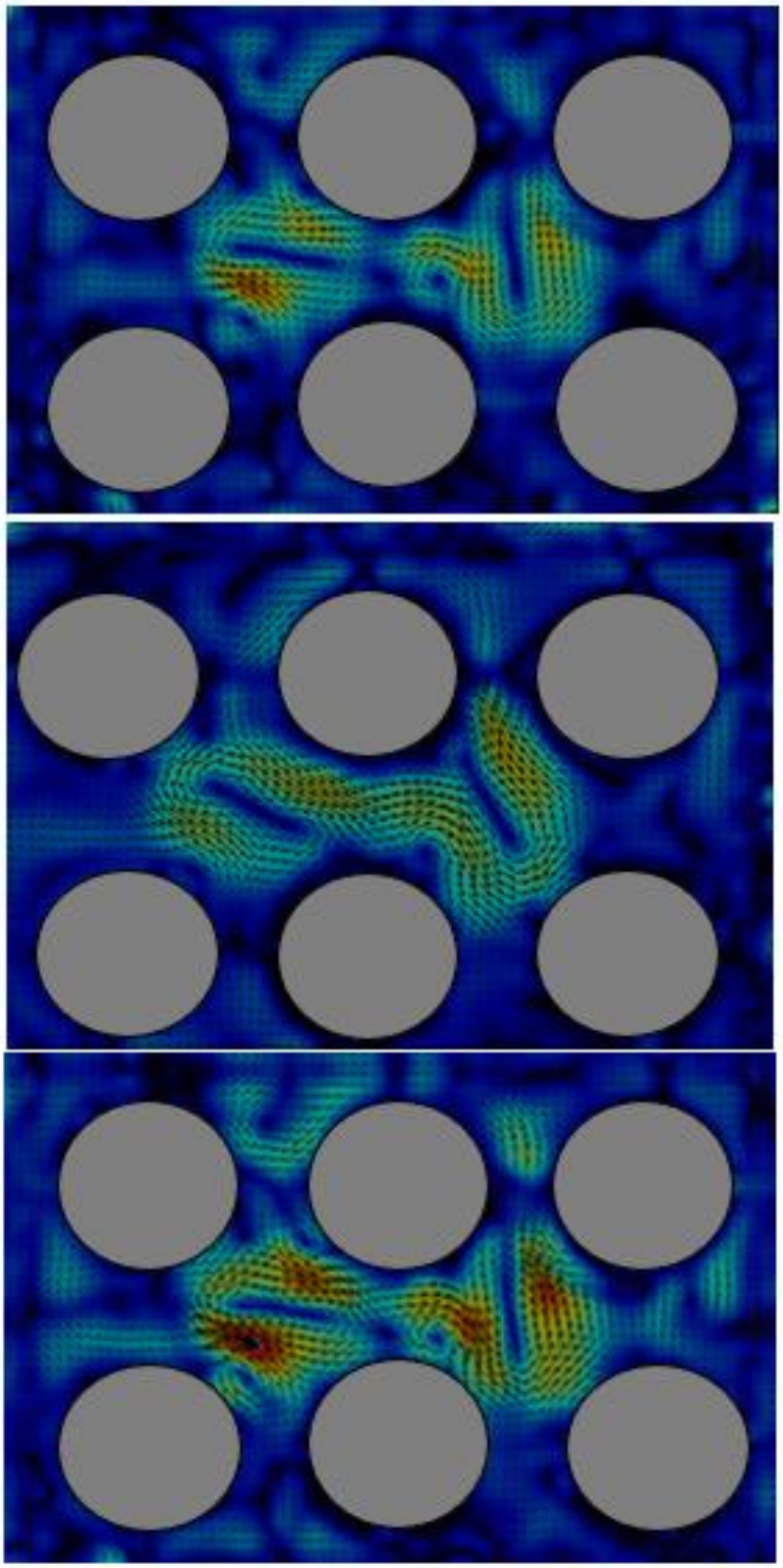

Figure 3. 3 (b) Lateral velocity flow field by PIV experiment, Z/Dh = 1, 2, and 3 for FSV

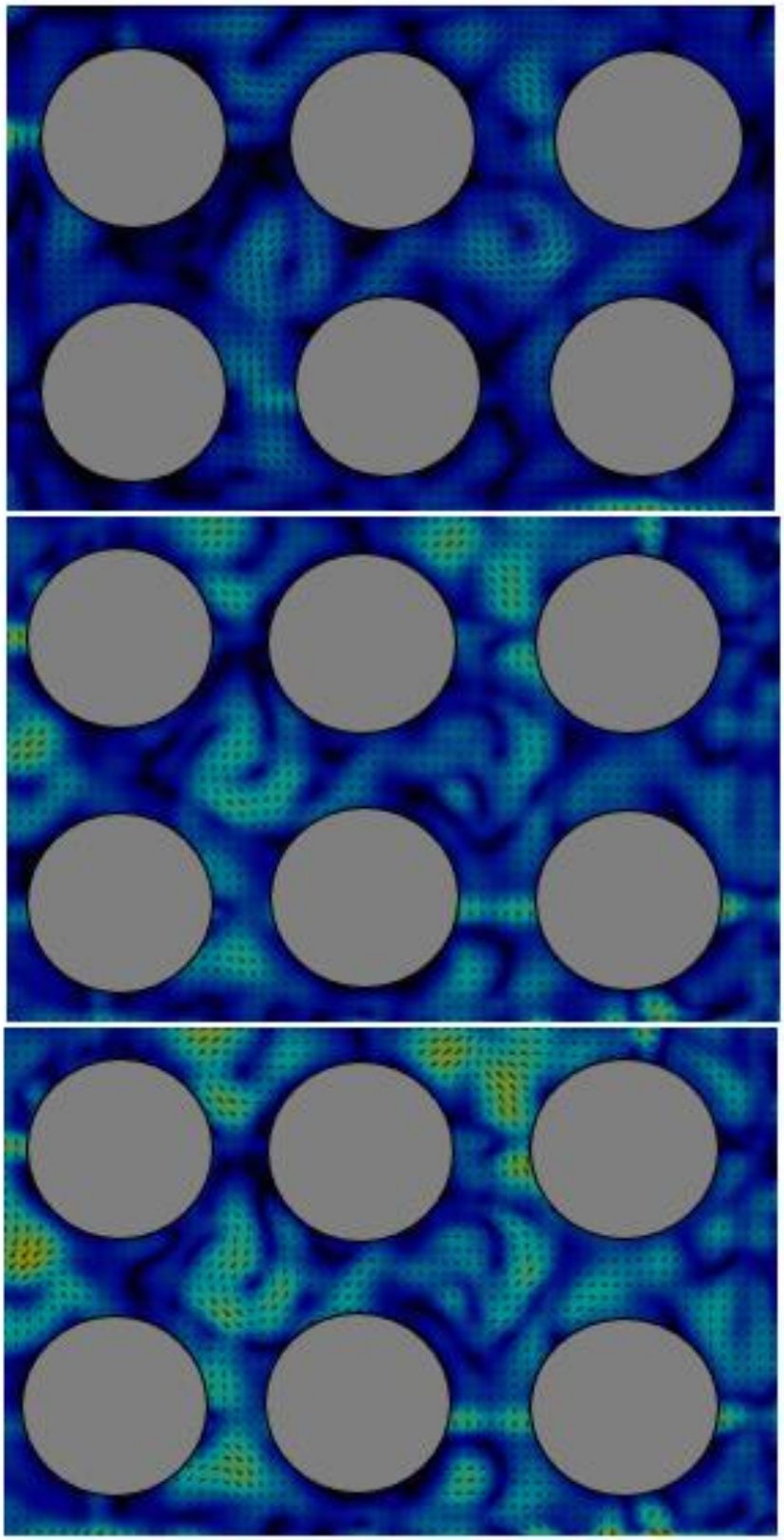

Figure. 3. 3 (c) Lateral velocity flow field by PIV experiment, Z/Dh = 1, 2, and 3 for RFV

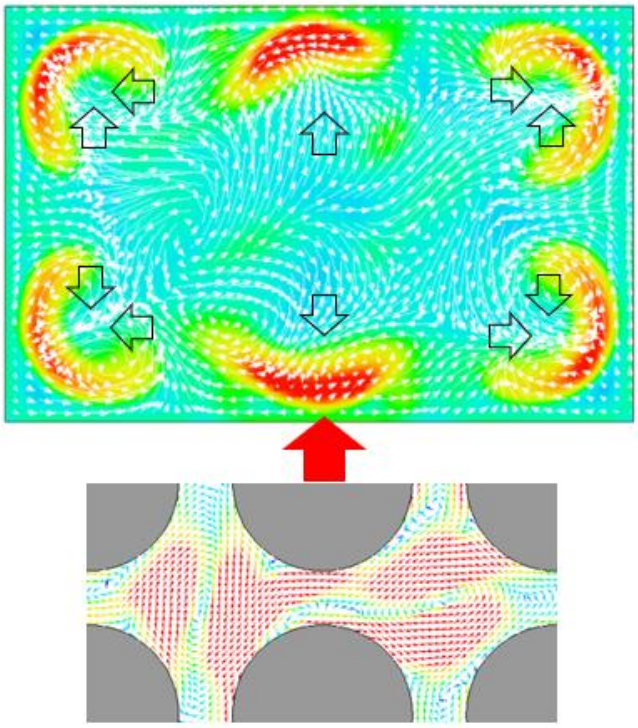

(a) FSV

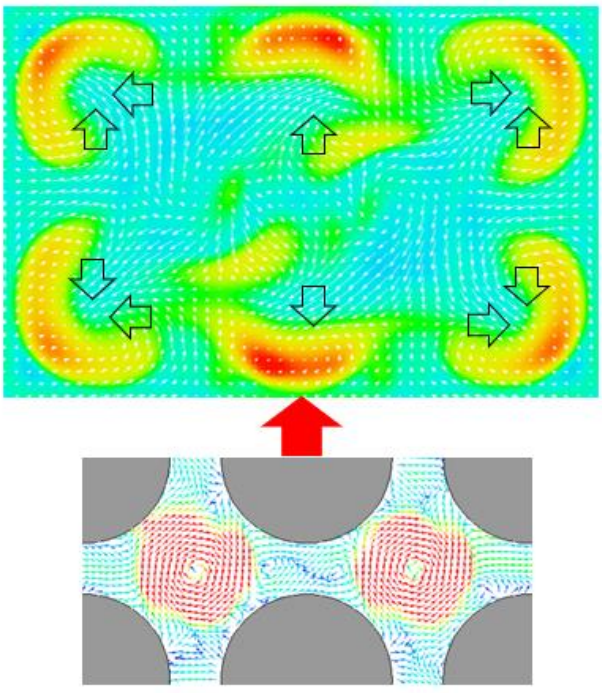

(b) RFV

Figure. 3. 4 Turbulent intensity by CFD analysis, (Q=145 lpm, v=0.7 m/s, Re=12,750)

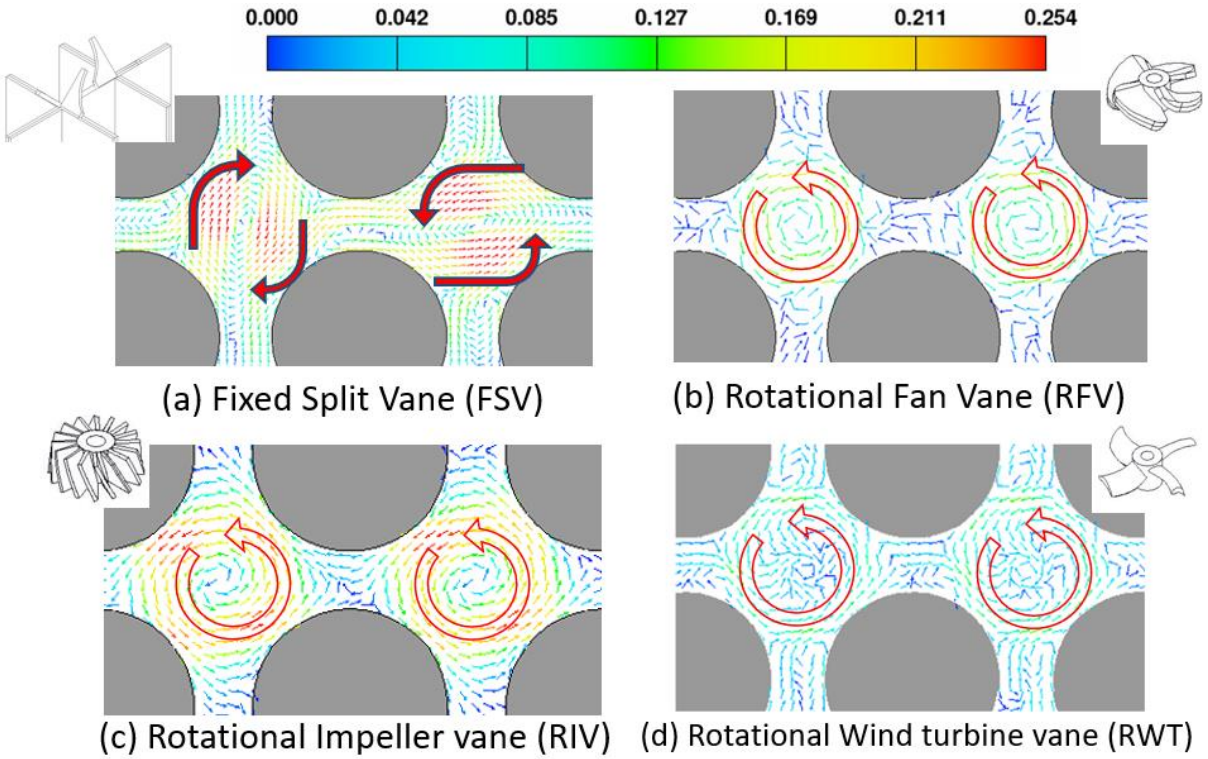

Figure. 3. 5 2D-Flow field with lateral velocity vector (m/s), Rotational mixing vane

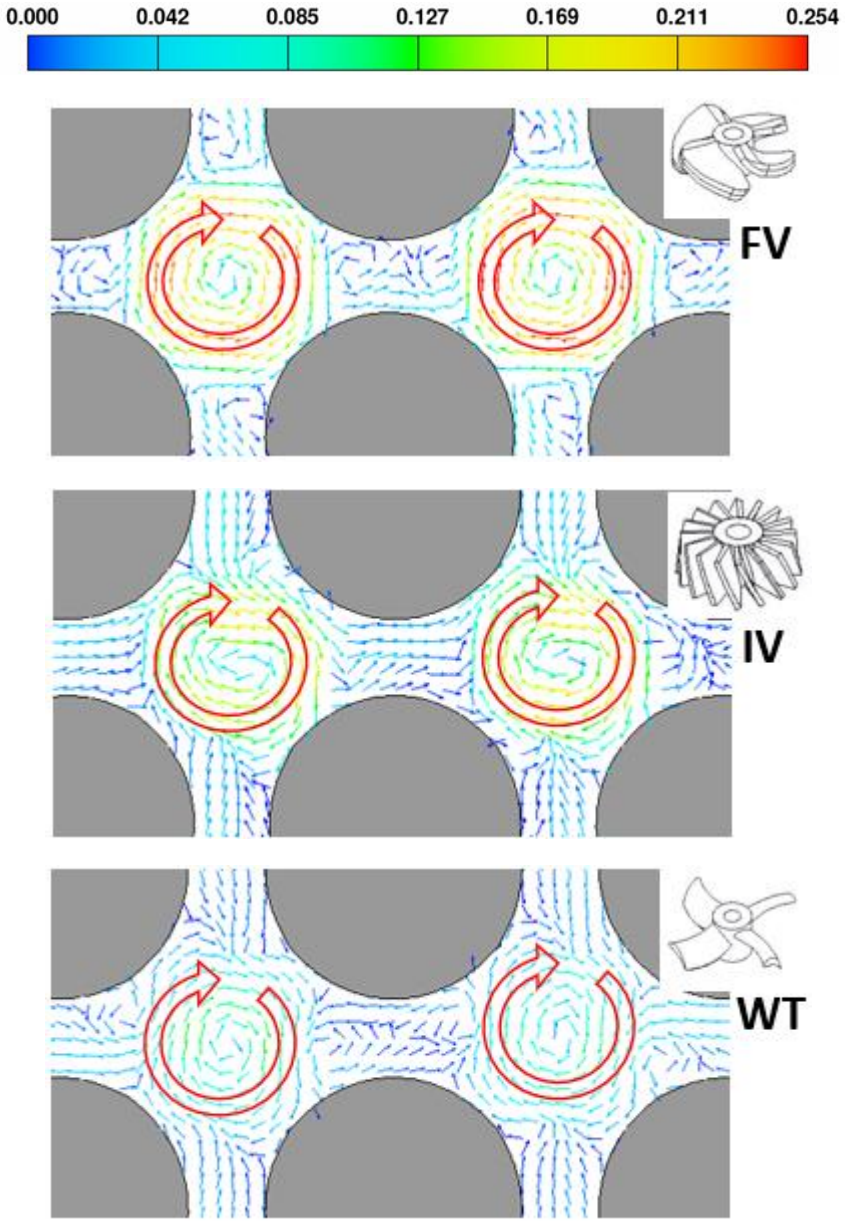

Figure. 3. 5 (b) 2D-Flow field with lateral velocity vector (m/s), Fixed mixing vane

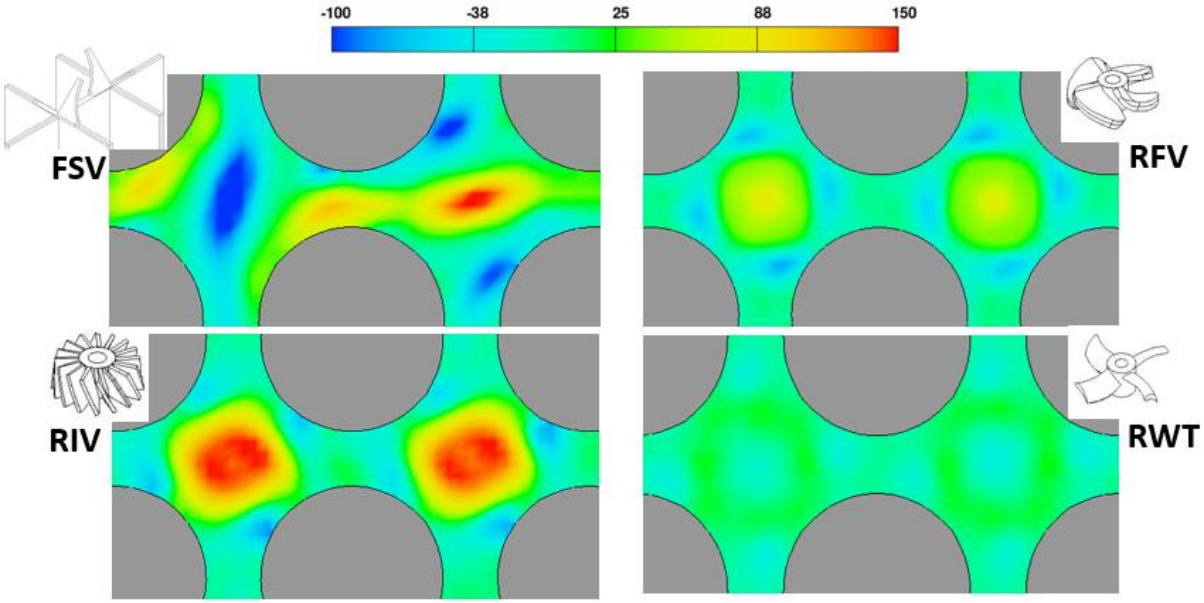

Figure. 3. 6 (a) 2D vorticity field by CFD analysis, (Q=145 lpm, v=0.7 m/s, Re=12,750)

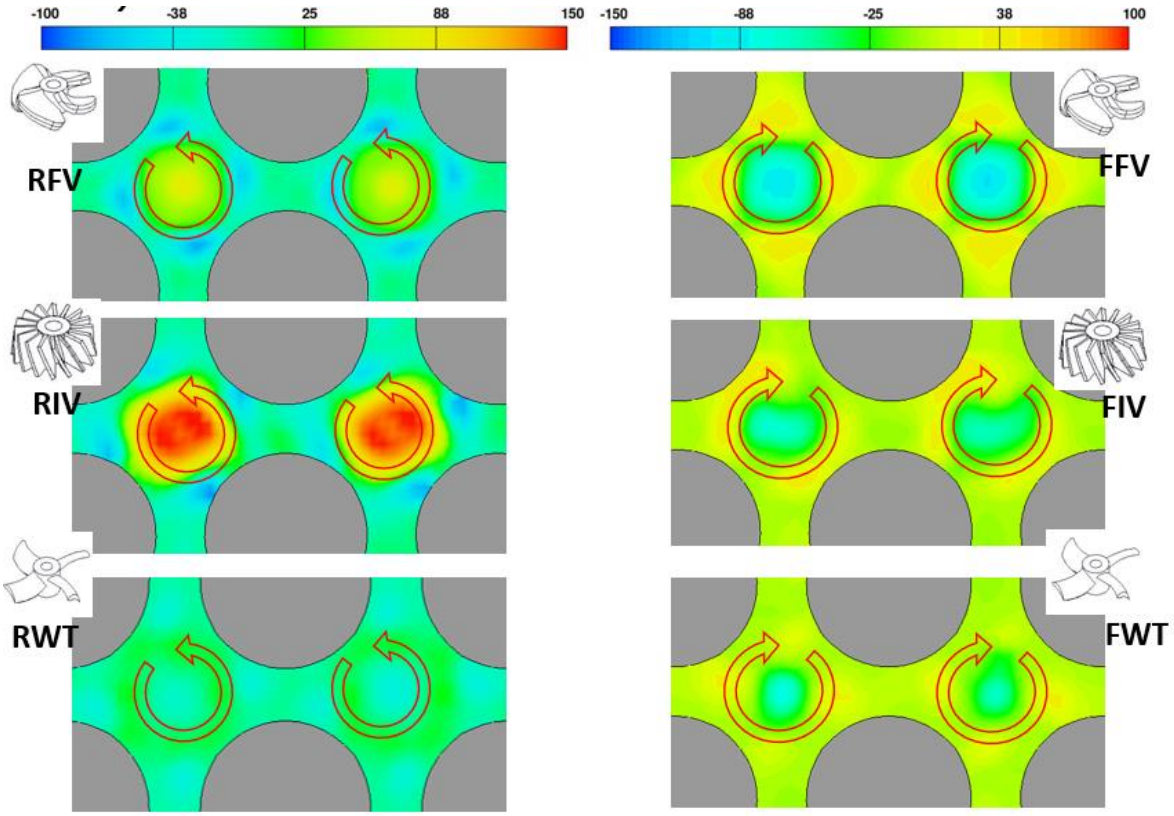

Figure. 3. 6 (b) 2D vorticity field by CFD analysis, (Q=145 lpm, v=0.7 m/s, Re=12,750)

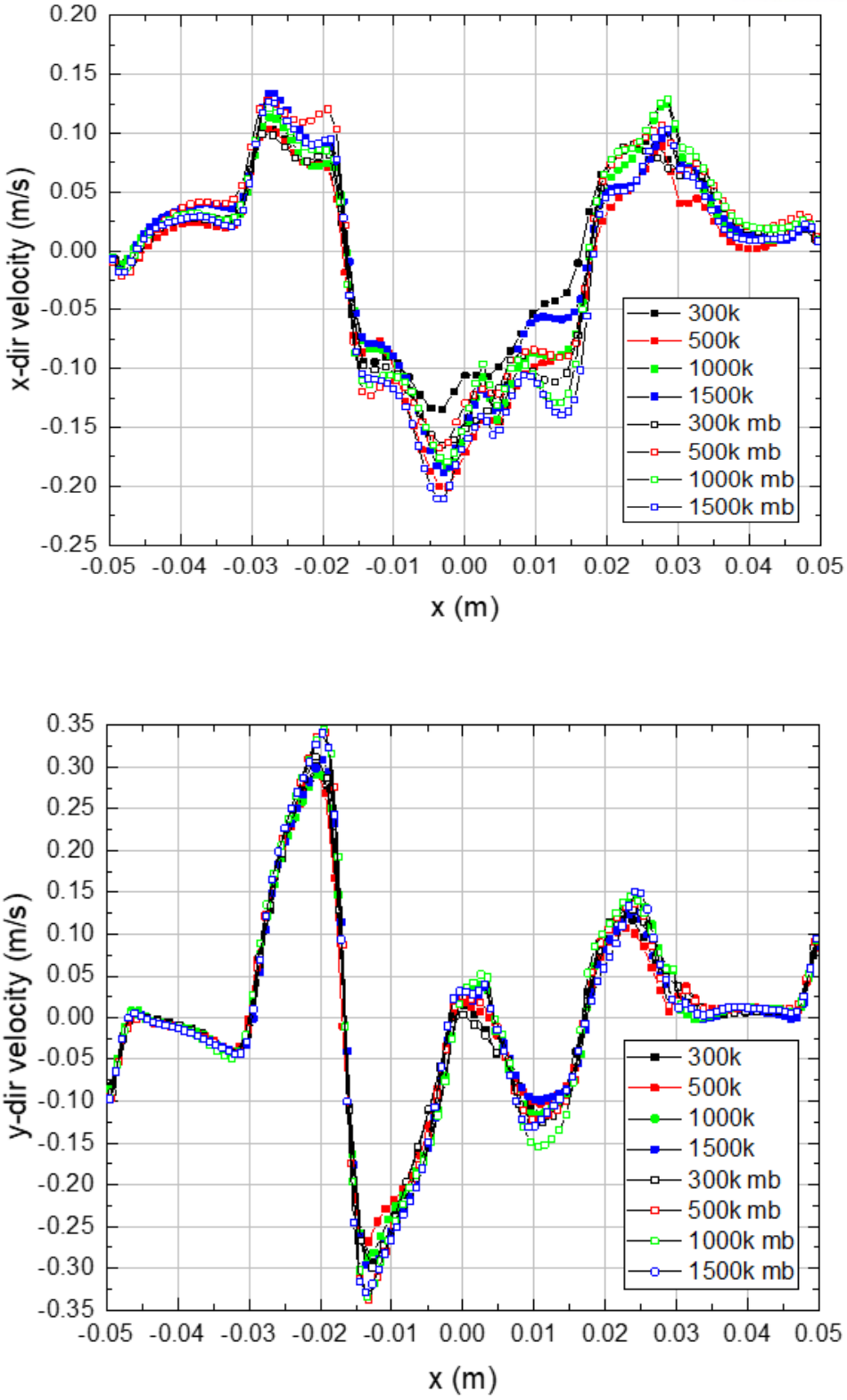

Figure. 3. 7 Lateral velocity distribution for mesh numbers, at Z/Dh = 1

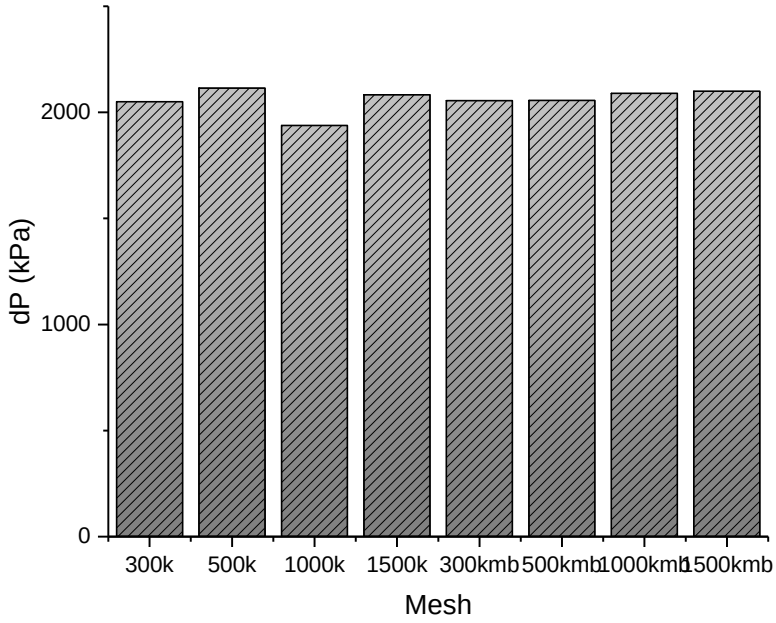

Figure. 3. 8 Pressure drop for mesh numbers, at $Z/D_h = 1$

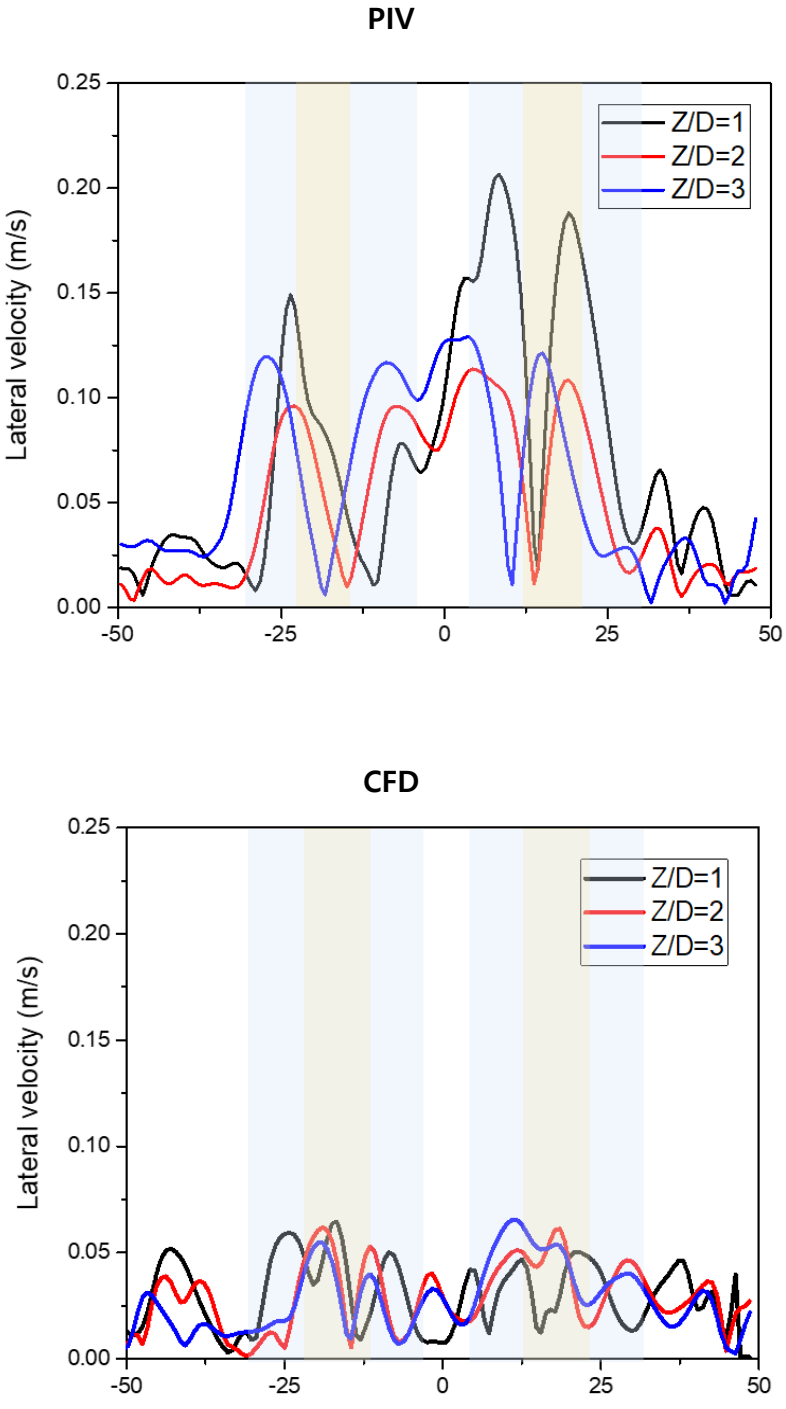

Figure. 3. 9 lateral velocity comparison at Z/D_h = 1, 2, 3

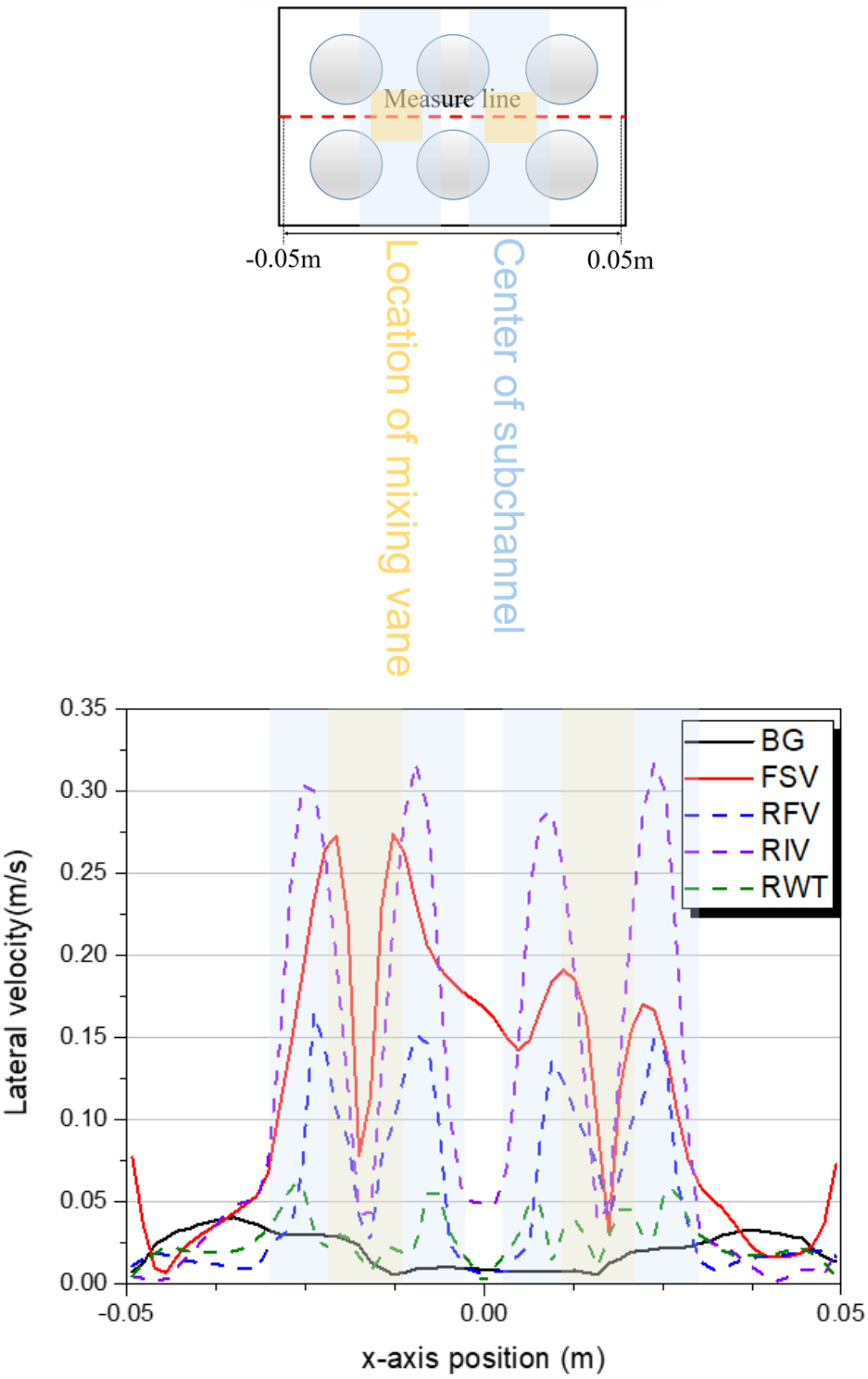

Figure. 3. 10 Lateral velocity distribution, Q=145 lpm, Re=12,750, $Z/D_h = 1$

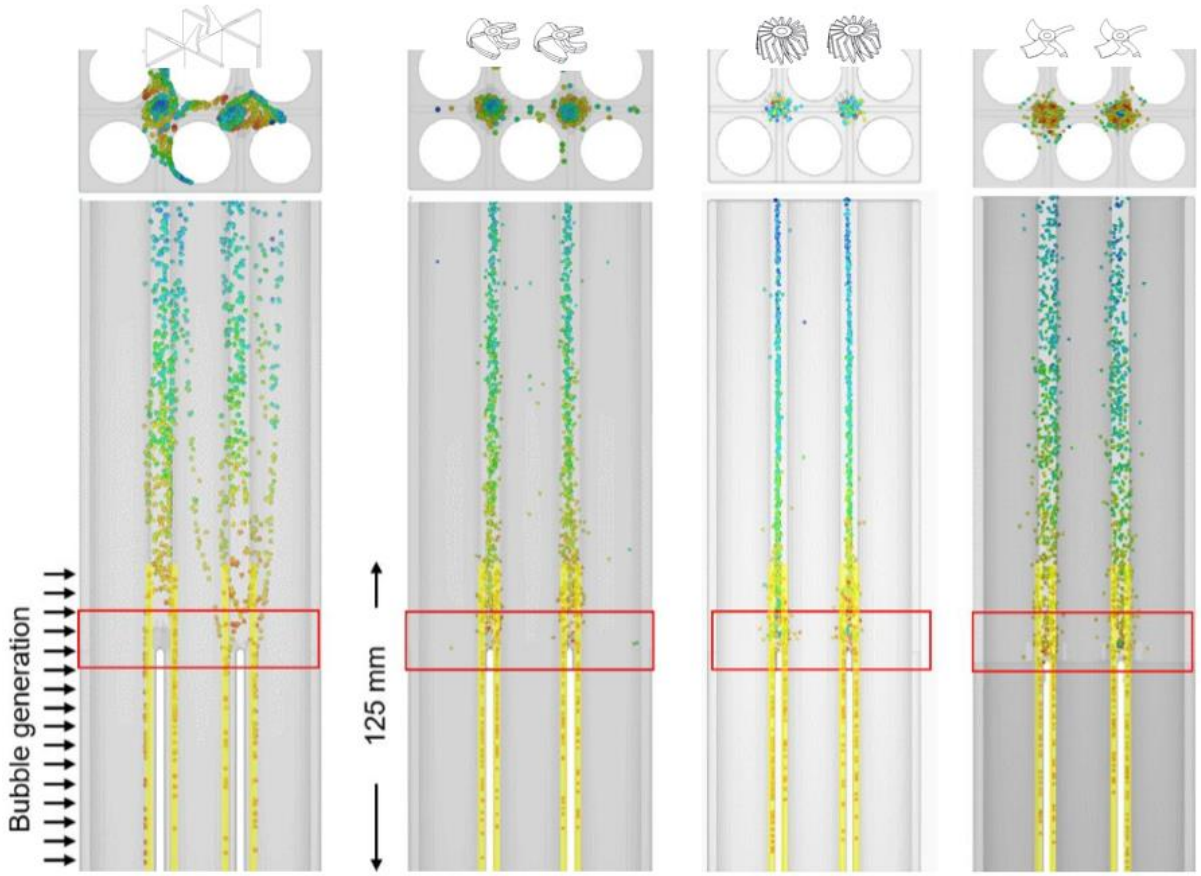

Figure. 3. 11 Bubble generation test in CFD analysis, Q=145 lpm

Table. 3. 1 The area average lateral velocity for each mixing vane type

	BG	FSV	RFV	RIV	RWT
Lateral velocity [m/s]	0.0214	0.122	0.055	0.125	0.028

Table. 3. 2 The area average vorticity for each mixing vane type

	BG	FSV	RFV	RIV	RWT
Vorticity [1/s]	-	47.7	24.7	64.6	7.41

Table. 3. 3 The pressure drop evaluation for experiment test section

	Differential pressure [Pa]	dP / dP_0	Friction Factor
BG	410 Pa	1	0.001232
FSV	425 Pa	1.037	0.001277
RFV	410 Pa	1.000	0.001232

Table. 3. 4 The pressure drop evaluation for CFD analysis using FLOW-3D

Mixing vane	Differential pressure [Pa]	dP / dP_0	Friction Factor
BG	206.2 Pa	1	0.000620
FSV	211.4 Pa	1.025	0.000635
RFV	209.9 Pa	1.018	0.000631
RIV	207.0	1.004	0.000622
RWT	197.9 Pa	0.96	0.000594

Chapter 4. CONCLUSION AND RECOMMENDATION

4.1 Conclusion

The 3D printed mixing vane and spacer grid parts were manufactured with gypsum and metal. The rotational motion and attachment, and durability were tested as first stage of adopting in PWR. The rotational mixing vane (RV) provides swirl and cross flow, with CHF enhancement and pressure drop reduction with flow-driven rotational motion. Fan vane (FV), impeller vane (IV), and wind turbine vane (WT) were designed as candidates of RV types. The flow-driven motion was validated with experimental method and CFD analysis with FLOW-3D code, by using General Moving Object (GMO) method. The cross flow and swirl were shown in mixing vane equipped 2×3 subchannel. PIV experiment and CFD analysis with FLOW-3D code showed the flow pattern. The mixing effect of flow-driven rotational mixing vanes was evaluated as swirl and cross flow driven by mixing vanes. For evaluating the mixing of the flow, swirl and cross flow were studied as lateral velocity, and vorticity. The fixed split vane (FSV) showed cross flow with cross flow offset, and Rotational mixing vane (RV) showed equalized swirl flow in the subchannel. The FSV and RIV showed the most lateral velocity, but RIV showed comparatively bigger vorticity, which simulate the centrifugal force. Also, the pressure drop was reduced with adopting RV in 2×3 subchannel. The CFD under-estimated for both velocity and pressure drop. Since bubbles converging to the center of the subchannel and by the centrifugal force of swirl, CHF enhancement is expected with mixing of coolant. Adopting the rotational mixing vane in the PWR could results enhancement of the heat transfer performance, safety margin and power uprate.

4.2 Recommendations

First, the 2.5 scaled up 2×3 subchannel could be extended with real scale 5×5 subchannel test section. The scale should be considered which affects to the friction and heat transfer performance.

Second, different rotational direction mixing vane installation would be designed for the test section. The swirl flow offset would enhance the mixing between the subchannel, and the cross flow shape would be studied with the direction and the place of RV in the extended subchannel.

Third, Heat transfer characteristics and thermal performance enhancement for experimental and numerical analysis would be validated in extended subchannel. For mixing parameter, HTC and mixing parameter as the ratio of HTC and pressure drop would be studied for further swirl and cross flow evaluation parameter.

Fourth, Optimized impeller vane for the RV model, with advanced spacer grid fixing the mixing vane inside the spacer grid would be suggested with patent. The FSV and RV could be installed in single spacer grid with advanced design. SprinKler Vane (KV) and sprinKler & Fan Vane (KFV) were also designed, expected to increase cross flow in the subchannel. However, the sprinkler types were leaved as further work due to the limitation of recent GMO technology. The 3D-printed mixing vane with metal structure was produced for FV, IV, WT, KV and KFV.

(a) Fan vane (b) Impeller vane (c) Wind turbine vane (d) Sprinkler vane

Figure. 4. 1 3D printed metal mixing vane

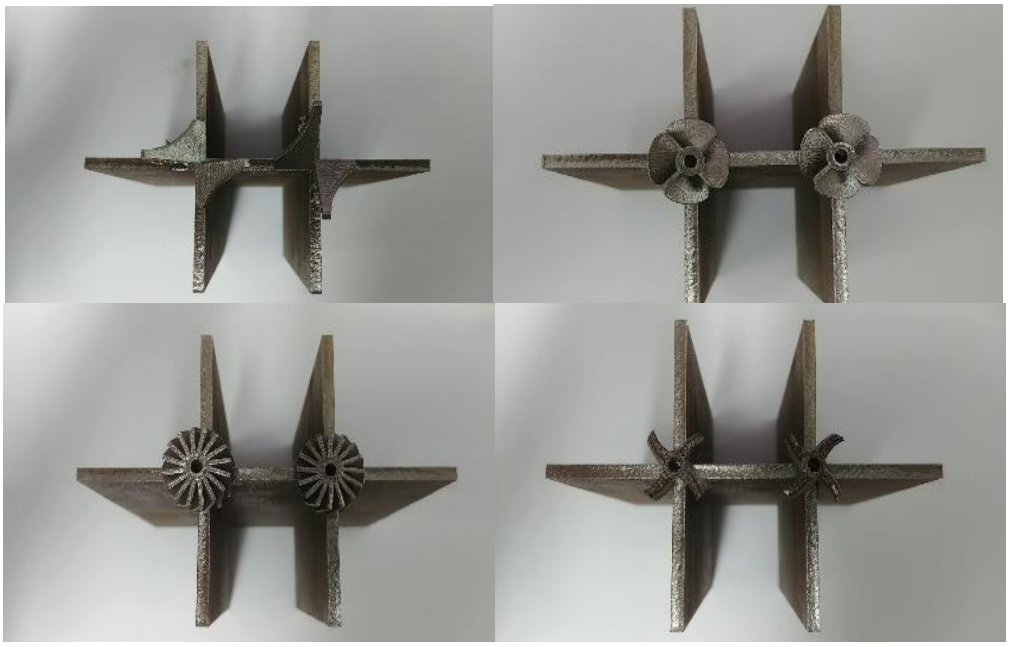

(a) Fixed split vane (b) Fan vane (c) Impeller vane (d) Wind turbine vane

Figure. 4. 2 3D printed mixing vane equipped spacer grid

References

1. M. E. Conner, Y. A. Hassan, E. E. Dominguez-Ontiveros, "Hydraulic benchmark data for PWR mixing vane grid," *Nuclear Engineering and Design,* **264**, pp. 97-102, (2013)
2. A. Kawahara, M. Sadatomi, Y. Hirakata, M. Endo, "Hydrogynamic effects of mixing vane attached to grid spacer on two-phase annular flow," *Nuclear Engineering and Design*, **310**, pp. 648-655 (2016)
3. A. Kawahara, M. Sadatomi, S. Imamura, Y. Shimoharai, Y. Hirakata, M. Endo, "Effects of grid spacer with mixing vane on entrainment and depositions in two-phase annular flows," *Nuclear Engineering and Technology*, **47**, pp. 389-397, (2015)
4. H. Seo., S. D. Park, S. B. Seo, H. Heo, I. C. Bang, "Swirling performance of flow-driven rotating mixing vane toward critical heat flux enhancement," *International Journal of Heat and Mass Transfer*, **89**, pp. 1216-1229 (2015)
5. S. K. Chang, S. K. Moon, W. P. Back, Y. D. Choi, "Phenomenological investigations on the turbulent flow structures in a rod bundle array with mixing devices," *Nuclear Engineering and Design*, **238**, pp. 600-609 (2008)
6. S. K. Chang, S. Kim, C. H. Song, "Turbulent mixing in a rod bundle with vaned spacer grids : OECD/NEA-KAERI CFD benchmark exercise test," *Nuclear Engineering and Design*, **279**, pp. 19-36, (2014)
7. M. Delgado, S. Lee, Y. A. Hassan, N. K. Anand, "Flow visualization study at the interface of alternating pitch tube bundles in a model helical coil steam generator using particle image velocimetry," *international Journal of Heat and Mass Transfer,* **122**, pp. 614-628, (2018)
8. Y. S. Tseng, Y. M. Ferng, C. H. Lin, "Investigating flow and heat transfer characteristics in a fuel bundle with split-vane pair grids by CFD methodology", *Annals of Nuclear Energy*, **64**, pp. 93-99, (2014)
9. M. E. Conner, E. Baglietto, A. M. Elmahdi, "CFD methodology and validation for single-phase flow in PWR fuel assemblies," *Nuclear Engineering and Design*, **240**, pp. 2088-2095, (2010)
10. C. m. Lee, Y. D. Choi, "Comparison of thermos-hydraulic performances of large scale vortex flow (LSVF) and small scale vortex flow (SSVF) mixing vanes in 17× 17 nuclear rod bundle," *Nuclear Engineering and Design,* **237,** pp. 2322-2331, (2007)
11. M. Endo, W. Takaki, D. Nishioka, Y. Hirakata, A. Kawahara, M. Sadatomi, "Effects of Mixing-vane Attached to Grid Spacer on Pressure Drop and Deposition Rate in BWR Simulated Channel," *Universal Journal of Mechanical Engineering,* **4**, pp. 57-62, (2016)
12. J. M. Gorman, E. M. Sparrow, S. Ilamaparuthi, W. J. Minkowycz, "Effect of fan-generated swirl on turbulent heat transfer and fluid flow in a pipe," *International Journal of Heat and Mass Transfer,* **95**, pp. 1019-1025, (2016)
13. I. C. Bang, S. H. Chang, "Flow mixing rotation vane attached in nuclear fuel spacer", *Korea Patent*, No. 10-0456500, (2004)
14. K. Miyazaki, K. Kawasue, L. Tao, S. Ohyama, "Calibration technique of PIV for distorted image using LCD", *IEEE Interantional symposium on industrial electronics,* Seoul, Korea, July 5-8, (2009)
15. Y. A. Hassan, R. E. Canaan, "Full-field bubbly flow velocity measurements using a multiframe particle tracking technique," *Experiments in Fluids*, **12**, pp. 49-60, (1991)
16. R. Theunissen, F. Scarano, M. L. Riethmuller, "Spatially adaptive PIV interrogation based on data ensemble," *Exp Fluids,* **48**, pp. 875-887, (2010)
17. S. Xianyang, D. Jie, "Design of multi-parameter target used in calibration of high precision CCD camera," *Optik*, **127**, pp. 548-552, (2016)
18. Flow science, flow-3D user Manual Version 3.2, (2009)
19. G. Wei, "A fixed-mesh method for general moving objects", *flow science Inc.,* **05**, (2005)

20. C. W. Hirt, B. D. Nichols, "Volume of Fluid (VOF) method for the dynamics of free boundaries", *Journal of computational physics,* **39**, pp. 201-225, (1981)
21. Nichols, B.D. and Hirt, C.W., "Methods for Calculating Multi-Dimensional, Transient Free Surface Flows Past Bodies," *Proc. First Intern. Conf. Num. Ship Hydrodynamics*, Gaithersburg, ML, Oct. 20-23, (1975)
22. Leonhard Meyer, "From discovery to recognition of periodic large scale vortices in rod bundles as source of natural mixing between subchannels – A review," *Nuclear Engineering and Design*, 240, pp. 1575-1588, (2010)
23. K. Podila, Y.F. Rao, M. Krause, J. Bailey, "A CFD simulation of 5 x 5 rod bundles with split-type spacers," *Progress in Nuclear Energy*, 70, pp. 167-175. (2014)

Acknowledgement (감사의 글)

열 여덟 해의 학업을 마치고 석사 학위를 받고 울산과학기술원 생활을 마무리하게 되었습니다. 어릴적부터 꿈 꿔온 연구자의 길에 한 걸음 더 다가서는 과정이었고 학업에 최선을 다한 시간이었다고 자부합니다. 논리와 창의, 진리의 상아탑에 오르기까지 긴 시간이었습니다.

세상 그 누구보다 소중한 가족들에게 진심으로 사랑한다는 말을 전하며 감사의 말을 시작하겠습니다. 영원한 내 편인 우리 가족. 아빠. 엄마. 동생. 모두 항상 사랑하고 항상 감사합니다. 가족들이 서로 맺어져 하나가 되어 있다는 것이 정말 이 세상에서의 유일한 행복이라고 합니다. 그리고 가정이란 어떠한 형태의 것이든 인생의 커다란 목표라고 합니다. 언제나 화목한 가족의 기운이 인생의 거름이 되었고 이렇게 아름다운 꽃을 피울 수 있었습니다. 최고로 사랑합니다.

먼저 학부생부터 석사 과정 연구실까지 지도교수님이신 방인철 교수님이자 기획처장님께 깊은 감사의 인사를 드립니다. 교수님의 지도와 가르침으로 원자력 학계에서 학업과 연구를 수행하며 많은 것을 배웠습니다. 교수님 기대에 부족한 모습도 있었지만 당신의 지도하에 많은 것을 배우고 무사히 원자력 공학 석사가 될 수 있었습니다. 감사합니다.
그리고 귀한 시간을 내서 석사 연구를 심사해준 심사위원들께 감사를 드립니다. 회전 혼합 날개의 기계적 거동에 대해 터빈의 대가로서 많은 조언을 주신 유춘상 교수님, 원자력 안전과 3D 프린트 부품에 대해 조언해 주신 이승준 교수님께 감사드립니다.

대학원 생활 2년간 동고동락해 온 열수력 랩실 식구들 한분 한분에게 감사의 말을 드립니다. 츤츤거리면서도 잘 가르쳐주신 한이형, 논리 설립과 학회 발표에 많은 조언을 해주신 경모형, 입학부터 함께 실험하고 야구하며 함께 뛴 석빈이형, 장치 설계 많이 도와주고 같이 맛있는 거 먹으러 많이 다닌 인국이형, 언제나 긍정적인 마음으로 힘이 돼 주고 함께 졸업하게 된 성보형, CFD 해석과 연구의 기본에 대해 많이 가르쳐준 영신이, 힘든 일 함께하고 학회에서도 함께 다녔던 효, 옆자리에서 랩실 생활 많이 가르쳐주고 노하우를 많이 알려주면서 동기처럼 친하게 지낸 빛과 어둠의 민호, 그리고 내 뒤에 들어온 우리 열수력 랩실 애기들 지용이, 도영이, 예영이, 동훈이. 함께해서 너무너무 즐거웠고 그간 말할 수 없을 만큼 고마웠습니다.

이하 연구를 도와 주신 분들에게 감사드립니다. 실험 장치와 실험 전부 책임져 주신 네오시스 이종수 사장님, 2년간 해석 시뮬레이션 프로그램 FLOW-3D를 가르쳐 주시고 언제나 성의있게 답변해주신 에스티아이씨앤디 민창원 과장님, PIV 실험장치 맡아 주신 엘투케이플러스 장선호 대리님, 3D 프린트 제작해주신 기기가공실 김진식 선생님, 행정업무 봐주신 이남기 선생님, 감사드립니다. 필드에서 밝은 햇살이 되어 준 벤치 클리어링 장영진 회장님, 김희중 선생님, 기민용 선생님, 구혁이형, 동근이, 그 외 멤버들 모두 감사드립니다.

살아오면서 지금의 저를 있게 해주신 분들에게 감사드립니다.
저를 가르쳐주신 은사님들 감사드립니다. 김건희 선생님, 박호식 선생님, 정지은 선생님, 그 외 일일이 언급 드리지 못했지만 저를 가르쳐주신 모든 은사님들께 감사드립니다.
음악과 창의성 함께해 온 분들에게 감사드립니다. 이인경 교수님, 강명미 조교님, 오연주 조교님께, 저는 공학도이지만 피아노 전공자들에게서 프로라는 것이 얼마나 무겁고 가치있는 것인지 많이 배웠고 책임감을 배웠습니다. 함께 가르친 학생 TA 유리, 선혜, 다은이, 함께 연주한 예진이, 우진이, 그 계기가 되어준 지원이, 모두 감사드립니다. 호주에서 만난 인연들, 그 6개월은 항상 잊지 못하고 있습니다. 연구에 대한 확신을 주고 어린 저를 인턴에서 연구자의 길로 이끌어주신 ANSTO의 Dr. Weijian Lu, Dr. Mark Ho et al., 시드니에서 따뜻하게 받아준 Roy and Gaynor Beadsworth, Aba, Abigail, Pepsi, and Oscar family, I really appreciate it and miss you all. 원자력협력재단 문인철 연구원님, 김영준 연구원님, 선배 봉호형, 동기 지민이, 함께 준비한 이레, 기회를 주셔서 감사합니다. 그리고 시드니한인연합교회에서 은혜주신 이봉우 목사님, 제임스형, 동현이형, 연희누나, 태수, 은주, 다미, 은석이, 홍열이. 그리고 좁은 세상 호주땅에서 만난 수정누나, 아영이, 수진이, 정민이, 재현이. 독립정신 답사단 현식이, 유경이, 지희. 제 인생의 다채로운 색깔 중에 아름다운 황금빛 크레마의 멋을 입혀주신 카페베네 고경주 사장님, 수빈이, 투썸 플레이스 박민영 점주님, 이동주 매니저님, 초롬이, 르미, 환상의 듀오 동진이, 커피 아젠다 사장님. 모두 감사합니다. 매순간 최선을 다하는 삶의 중요성을 가르쳐준 필름몰딩컴퍼니의 배수형 대표님, 수호형, 희동이형. 수고하셨습니다. 함께 복무한 Camp CarrollI의 허경원 상사님, SSG R. Hernandez, 범주형, 우현이형, 영광이형, 성환이형, 준희형, 태윤이형, 정수, 부엘이, 또한 함께한 귀랑이, 진홍이, 재현이형, 지훈이형. 단결. 감사합니다. 또다른 가르침을 준 하영이, 준영이, 고맙다. 삶의 다이나믹을 알려주신 베이스의 이재훈 선생님, 보컬 최구민 선생님, 고맙습니다.

또한 지금도 유니스트에서 학사학위를 수료한, 또는 현재 석 박사 학위 과정을 밟고 있는 친구들에게 감사와 응원을 보냅니다. 모아하임부터 대학원 내내 함께 멘탈 잡아주고 토론해 온 정현이, 그동안 룸메이트로 맛집 투어 다니고 라이프 밸런스를 함께 해 온 혁준이, 지금 룸메 성남이, 응원합니다. 울산 땅 처음 왔을 때부터 함께 해 온 창윤이형, 태희형, 상필이형, 재경이형, 종환이형, 상윤이, 윤석이, 의상이, 성현이, 승준이, 영오, 영수, 호석이, 창현이, 기도. 후배이자 동생들, 민곤이, 원식이. 모아하임의 정수, 규빈이, 우석이, 뜨겁고 좋은 추억 고맙다. 모두 자대에서 또는 타대에서 무사히 학위 마치기 바란다. 너무나도 애정하는 유니스트 로켓츠 멤버들 고맙습니다. 동아리 후배이자 원자력 학과 후배로 수많은 시간을 함께한 승록이, 우리 팸 원재, 재민이, 혜진이, 다빈이, 기헌이, 창단멤버 성훈이형, 익재형, 태정이, 영재, 승진이, 병일이, 용진이, 한빈이, 함께한 선수와 매니저들, 광원이형, 명훈이형, 창배형, 대현이, 재철이, 호재, 정태, 금택이, 도현이, 동현이, 준우, 종찬이, 지수, 민정이, 동원이, 진홍이, 행복했습니다.

멀리서 힘과 응원이 되어준 친구들에게도 따로 감사합니다. 어느 곳에 있어도 다른 삶을 살아도 언제나 함께인 베프 상훈이, 민석이, 내일로 혹은 그 전부터 그리고 앞으로도 함께 할 아이헨불패의 여나 성엽이, 식라인 원식이. 빛나는 학창시절의 별들, 상원반의 현준이, 한별이, 덕영이, 꿈을

가진 소년들, LOS 지성이, 해솔이, 재선이. 우리 오래방 패밀리들 20살의 그날들 너무 즐거웠다. 고삼을 함께 해 온 민재, 덕언이, 동민이. 우리 월촌초 야구 멤버 희문이, 동완이, 보규, 지훈이, 찬호. 너희와 운동장에서 함께한 그 시절의 즐거움은 평생 다신 없을 것 같다. 그리고 10 화석들 명준이, 재식이, 성소, 언제 다시 그때처럼 놀아볼 수 있을까. 오랜 친구, 주현이, 영두, 슬기, 원석이, 은택이, 기범이, 기헌이, 기태, 형진이, 그 외 모든 친구들아, 어린 시절 함께여서 고마웠다.

함께 걸어 온 원자력학과 학생들, 감사합니다. 아귀 맞게 함께 한 동현이 즐거웠고, 명규형, 관윤이형, 유경이, 지예, 윤주, 지현이, 도훈이, 병관이, 지속가능한 미래를 위해 발전합시다.

태어난 순간부터 인연을 함께한 사촌들, 미선누나, 재복이형, 재선이형, 선욱이형, 영하누나, 병훈이형, 지은누나, 수연누나, 만기형, 전민누나, 지석이형, 지민이, 정석이, 다들 고마워요. 그리고 언급하지 못한 모든 친척분들 고마워요.

마지막으로 그 동안 함께해 온 울산 식구들, 민서누나, 용준이형, 수지누나, 정민누나, 현정누나, 창훈이형, 원재형, 주경이형, 효원이형, 현주형, 유수형, 장후형, 옥이, 깜이. 당신들이 일깨워준 자신감이 저를 태우는 연료가 될 수 있었고 덕분에 제가 살 수 있었습니다. 정말 감사합니다.

보름달을 바라보던 긴 밤을 지나 처음 걸은 가로등 불빛 아래 유니스트의 길은 아직 덜 닦인 진흙길이었습니다. 봄 소나기 후 창가의 밝은 햇살, 모두 녹아내렸다가 다시 얼어붙는 가막못의 겨울, 선물처럼 저물던 빨간 목도리의 노을, 잠 못 드는 환한 백야, 반짝이는 셋잇단음표의 유성우, 흰 오리의 안식일, 선명한 일곱빛깔 무지개와, 보랏빛 자카란다 나무 아래에서 들은 남십자성의 아리아, 항상 푸른 유니스트의 운동장과 꺼지지 않는 불빛, 연구실에서 키운 알록달록 구피들과 빨간 베타, 그리고 깊을수록 짙어지는 낮은 하늘과 높은 바다의 비취색까지. 돌이켜보면 세상은 항상 눈부시게 환하고 정채가 있었습니다. 긴 대학원 생활을 지나 밖으로 나온 오늘도 눈부시게 밝은 바람을 느낍니다.

20대의 시작과 함께한 유니스트에서 유종의 미를 거둘 수 있어 기쁩니다. 유니스트에서 얻은 소중한 기억들과 함께입니다. 살아오면서 얻은 기억들은 영원히 변하지 않을 경험으로 새겨집니다. 지금까지 열심히 살아온 스스로에게 대견하다고 말해주고 싶습니다.
운명이란 참 재밌습니다. 아주 가끔보다 더 자주 운명은 문을 두드리는 것처럼 보였습니다. 예정된 운명의 길에 올라서기 시작한 후 끊임없이 걷다 보면 언젠가 목적지에 도달해 있는 자신을 발견하게 되는 것 같습니다. 언제부터인가 올라서 걸어온 이 길에서 하나의 목적지에 도달했습니다. 다음 도착지가 어디인지 지금 육안으로는 보이지 않지만, 길을 따라 걷다 보면 또다른 운명을 마주하게 될 거라 믿습니다. 제 앞에 펼쳐진 그 길을 밝고 굳은 마음으로 힘차게 걸어가겠습니다.